Mantle wedge exhumation beneath the Dora-Maira (U)HP dome unravelled by local earthquake tomography (Western Alps)

Stefano Solarino, Marco Malusà, Elena Eva, Stéphane Guillot, Anne Paul, Stéphane Schwartz, Liang Zhao, Coralie Aubert, Thierry Dumont, Silvia Pondrelli, et al.

Pre-print

Solarino S., Malusa M. G., Eva E., Guillot S., Paul A. et al. (2018)

Mantle wedge exhumation beneath the Dora-Maira (U) HP dome unravelled by local earthquake tomography (Western Alps).

Lithos, 296, 623-636.

https://doi.org/10.1016/j.lithos.2017.11.035

Mantle wedge exhumation beneath the Dora-Maira (U)HP dome unravelled by local earthquake tomography (Western Alps)

Stefano Solarino[1], Marco G. Malusà[2], Elena Eva[1], Stéphane Guillot[3], Anne Paul[3], Stéphane Schwartz[3], Liang Zhao[4], Coralie Aubert[3], Thierry Dumont[3], Silvia Pondrelli[5], Simone Salimbeni[5], Qingchen Wang[4], Xiaobing Xu[4], Tianyu Zheng[4], Rixiang Zhu[4]

[1] *Istituto Nazionale di Geofisica e Vulcanologia, CNT, Genova, Italy*

[2] *Department of Earth and Environmental Sciences, University of Milano-Bicocca, Milano, Italy*

[3] *Univ. Grenoble Alpes, Univ. Savoie Mont-Blanc, CNRS, IRD, IFSTTAR, ISTerre, Grenoble, France*

[4] *Institute of Geology and Geophysics, Chinese Academy of Sciences, Beijing, China*

[5] *Istituto Nazionale di Geofisica e Vulcanologia, Bologna, Italy*

Authors for correspondence : S. Solarino and M.G. Malusà (stefano.solarino@ingv.it; marco.malusa@unimib.it)

Abstract

In continental subduction zones, the behaviour of the mantle wedge during exhumation of (ultra)high-pressure [(U)HP] rocks provides a key to distinguish among competing exhumation mechanisms. However, in spite of the relevant implications for understanding orogenic evolution, a high-resolution image of the mantle wedge beneath the Western Alps is still lacking. In order to fill this gap, we perform a detailed analysis of the velocity structure of the Alpine belt beneath the Dora-Maira (U)HP dome, based on local earthquake tomography independently validated by receiver function analysis. Our results point to a composite structure of the mantle wedge above the subducted European lithosphere. We found that the Dora-Maira (U)HP dome lays directly above partly serpentinized peridotites (Vp ~7.5 km/s; Vp/Vs = 1.70-1.72), documented from ~10 km depth down to the top of the eclogitized lower crust of the European plate. These serpentinized peridotites, possibly formed by fluid release from the subducting European slab to the Alpine mantle wedge, are juxtaposed against dry mantle peridotites of the Adriatic upper plate along an active fault rooted in the lithospheric mantle. We propose that serpentinized mantle-wedge peridotites were exhumed at shallow crustal levels during late Eocene transtensional tectonics, also

triggering the rapid exhumation of (U)HP rocks, and were subsequently indented under the Alpine metamorphic wedge in the early Oligocene. Our findings suggest that mantle-wedge exhumation may represent a major feature of the deep structure of exhumed continental subduction zones. The deep orogenic levels here imaged by seismic tomography may be exposed today in older (U)HP belts, where mantle-wedge serpentinites are commonly associated with coesite-bearing continental metamorphic rocks.

Keywords: continental subduction; ultra-high-pressure metamorphism; mantle wedge exhumation; peridotite serpentinization; local earthquake tomography; Western Alps

Highlights:

- High-resolution image of the seismic velocity structure of the Alpine mantle wedge
- First geophysical evidence of mantle-wedge exhumation during continental subduction
- Mantle wedge exhumation is favoured by upper plate divergent motion

1. Introduction

Exhumed (ultra)high-pressure [(U)HP] rocks bear compelling evidence of the interaction between subducting plates and the overlying mantle wedge (Carswell and Compagnoni, 2003; Hacker et al., 2006; Ferrando et al., 2009; Scambelluri et al., 2010; Deschamps et al., 2013; Gilotti, 2013). However, the role played by the mantle wedge during (U)HP rock exhumation is still poorly understood. Some numerical models point to a negligible mantle involvement during exhumation (Yamato et al., 2008; Butler et al., 2013), whereas other models suggest that mantle rocks may be strongly involved, and may follow the exhumation path of buoyant (U)HP rocks towards the Earth's surface (Schwartz et al., 2001; Petersen and Buck, 2015). The behaviour of the mantle wedge during (U)HP rock exhumation may thus provide a key to discriminate among competing exhumation models (e.g., Agard et al. 2009; Guillot et al., 2009a; Liou et al., 2009; Warren, 2013).

In the Cenozoic metamorphic belt of the Western Alps, the geologic record of subduction and exhumation is exceptionally well preserved (e.g., Lardeaux et al., 2006; Malusà et al., 2011), but a high-resolution image of the mantle wedge is still lacking. A detailed analysis of the seismic velocity structure beneath the Dora-Maira (U)HP dome, where coesite attesting deep continental subduction was first described three decades ago (Chopin, 1984), may thus provide new insights on the ongoing debate concerning the mechanisms triggering the exhumation of (U)HP rocks (e.g., Jolivet et al., 2003; Schwartz et al., 2001; Agard et al., 2009; Little et al., 2011; Butler et al., 2013; Malusà et al., 2015; Ducea, 2016). Moreover, this kind of analysis may provide new interpretation keys to understand the field relationships between mantle-wedge rocks and continental (U)HP rocks in deeply unroofed pre-Cenozoic orogenic belts (e.g., van Roermund, 2009; Scambelluri et al., 2010), where the geophysical record of subduction and exhumation is no longer preserved (e.g., Zhao et al. 2017).

In this article, we exploit a comprehensive seismic dataset, also including anomalously deep earthquakes (Eva et al., 2015), to derive a local earthquake tomography model of the mantle wedge beneath the Dora-Maira (U)HP dome, which is then compared with the results provided by receiver function analysis along the CIFALPS transect (China-Italy-France Alps seismic survey; Zhao et al., 2015). Our results indicate that part of the mantle wedge was metasomatized above the Alpine subduction zone, and subsequently exhumed at shallow depth beneath continental (U)HP rocks now exposed at the surface. This suggests that mantle-wedge exhumation may be a prominent feature of the deep structure of many (U)HP belts, which should be integrated in future theoretical models of continental subduction and (U)HP rock exhumation.

2. Tectonic framework

2.1 The orogenic wedge of the southern Western Alps

The Western Alps are the result of oblique subduction of the Alpine Tethys under the Adriatic microplate since the Late Cretaceous, followed by continental collision between the Adriatic and

European paleomargins during the Cenozoic (Coward and Dietrich, 1989; Dewey et al., 1989; Lardeaux et al., 2006; Handy et al. 2010; Malusà et al., 2016a). The resulting slab structure is still largely preserved (Zhao et al., 2016a), as well as the orogenic wedge formed atop the European slab (Lardeaux et al., 2006; Beltrando et al., 2010; Malusà et al., 2011). In the southern Western Alps, along the CIFALPS transect (X-X' in Fig. 1), the Alpine orogenic wedge mainly consists of rocks derived from the Piedmont ocean-continent transition and from the adjoining European paleomargin (Lemoine et al., 1986; Dumont et al., 2012). The external zone, exposed to the west of the Frontal Pennine Fault (FPF in Fig. 1), includes the Pelvoux and Argentera basements and their deformed Meso-Cenozoic sedimentary cover sequences (Ford et al., 2006), which record a transition from thin-skinned to thick-skinned compressional tectonics during the Neogene (Schwartz et al., 2017). East of the Frontal Pennine Fault, in the Alpine metamorphic wedge, the Briançonnais nappe stack (Br in Fig. 1) mainly consists of Upper Paleozoic to Mesozoic metasediments and underlying pre-Alpine basement rocks that underwent subduction starting from the Paleocene, and were later exhumed in the Eocene - early Oligocene (Malusà et al., 2002, 2005a; Ganne et al., 2007; Lanari et al., 2014). The Briançonnais nappe stack forms the core of the present-day Alpine fan-shaped structure (Michard et al., 2004) that was overprinted by a dense network of extensional faults during the Neogene (Sue et al., 2007; Malusà et al., 2009). The eastern part of the fan is formed by oceanic metasediments of the Schistes lustrés complex (SL in Fig. 1; Lemoine et al., 1986; Lagabrielle and Cannat, 1990), including boudinaged decametre-to-kilometre-sized ophiolitic bodies that were deformed and metamorphosed during Alpine subduction under blueschist to transitional blueschist–eclogite facies conditions (Agard et al., 2002; Tricart and Schwartz, 2006; Schwartz et al., 2009) (Fig. 2A). A ductile normal fault (DF1 in Fig. 2A; Ballèvre et al., 1990) separates the Schistes lustrés complex from the Viso metaophiolites (Vi in Fig. 1; Lombardo et al., 1978; Angiboust et al., 2012), representing major imbricated remnants of the Tethyan oceanic lithosphere that were deformed and metamorphosed under eclogite facies conditions during the Eocene (Duchêne et al., 1997; Schwartz et al., 2000; Rubatto and Hermann, 2003). Another ductile normal fault (DF2 in

Fig. 2A; Blake and Jayko, 1990) separates the Viso eclogites from the underlying stack of deeply subducted continental basement slices referred to as the Dora-Maira (U)HP dome (DM in Fig. 1; Henry et al., 1993; Michard et al., 1993), which also includes the coesite-bearing Brossasco-Isasca eclogitic unit (black star in Figs. 1 and 2A; Chopin et al., 1991; Compagnoni and Rolfo, 2003). Along the boundary with the Po Plain, the CIFALPS transect crosses the southern tip of the Lanzo massif (La in Fig. 1; Boudier, 1978; Piccardo et al., 2007), an eclogitized mantle slice separated from the Dora-Maira dome by a near-vertical active fault system rooted in the upper mantle (Rivoli-Marene deep fault - RMF in Fig. 1) at the southward prolongation of the Insubric Fault (Eva et al. 2015; Malusà et al., 2017). The Lanzo massif consists of slightly serpentinized spinel plagioclase peridotites surrounded by a 3–5 km thick envelope of foliated serpentinites (Müntener et al., 2004; Debret et al., 2013), and records a high-pressure metamorphic peak of early Eocene age (Rubatto et al., 2008). Beneath the Po Plain, the complex transition zone between the Adriatic upper plate and the Apennines, also involving rotated fragments of the Alpine orogenic wedge (Maffione et al., 2008; Eva et al. 2015), is mainly covered by thick Cenozoic to Quaternary sedimentary successions.

2.2 The Dora-Maira (U)HP dome

The Dora-Maira (U)HP dome is exposed all along the internal side of the southern Western Alps (Chopin et al., 1991; Lardeaux et al., 2006) (Fig. 1). To the west of Torino, it is juxtaposed against the Lanzo massif along the Lis-Trana deformation zone (Perrone et al., 2010), possibly representing a shallow splay of the Rivoli-Marene deep fault (Eva et al., 2015). To the south, it is partly buried by the sedimentary successions of the Po Plain (Fig. 1), and is exposed as a half-dome including coesite-bearing eclogitic rocks (Brossasco-Isasca unit) sandwiched between quartz-eclogite facies rocks, above, and blueschist facies rocks, below (Compagnoni et al. 1995; Avigad et al., 2003; Compagnoni and Rolfo, 2003) (Fig. 2A). The Brossasco-Isasca unit is a coherent continental crust sliver composed of granitic gneisses (Lenze and Stöckhert, 2007), whiteschists (Chen et al., 2017), mafic eclogites (Groppo et al., 2007) and impure marbles (Ferrando et al.,

2017). It was subducted to depths greater than ~100 km by the late Eocene (e.g., Chopin et al., 1991; Rubatto and Hermann, 2001; Hermann, 2003), and was exhumed close to the Earth's surface by the early Oligocene, at rates faster than subduction rates (Rubatto and Hermann, 2001; Malusà et al., 2015), as confirmed by low-temperature thermochronology data (Gebauer et al., 1997; Tricart et al., 2007; Beucher et al., 2012). The overlying quartz-eclogite Venasca *p.p.* and Dronero units, including gneisses and metasediments derived from a Permian-Triassic detrital sequence, and the underlying blueschist-facies Sanfront-Pinerolo unit, consisting of orthogneisses and metasediments intruded by Permian diorites (Avigad et al., 2003), were piled up together with the Brossasco-Isasca and Viso units during late Eocene exhumation (Schwartz et al., 2009; Malusà et al., 2011), to became part of the Eocene Eclogite belt now exposed along the upper-plate side of the Western Alps (Fig. 1), at the rear of a lower-pressure Paleogene wedge (LP in Fig. 2B,C).

The structure and lithologic composition of the orogenic wedge beneath the Dora-Maira (U)HP dome is still largely unknown. The velocity structure provided by available seismic tomography models is well resolved only for the uppermost 15-20 km (Paul et al., 2001; Béthoux et al., 2007). Recent tectonic reconstructions postulated the occurrence of Briançonnais crust slivers down to depths greater than 30 km, and suggested that these slivers would be involved in an east-vergent backfold at the scale of the whole Eclogite belt (Schmid et al., 2017). However, the Dora-Maira dome shows no cartographic evidence of such large-scale backfolding, which is instead observed in the Monte Rosa dome (MR in Fig. 1) of the northern Western Alps, where late backfolding is possibly ascribed to progressive westward shifting of Adria indentation from the Central Alps to the northern Western Alps during the Neogene (Malusà et al., 2016b). As a matter of fact, alternative interpretations of the deep tectonic structure of the southern Western Alps are not adequately supported by geophysical data. This information gap has so far precluded a full understanding of the exhumation mechanisms that were active within the Alpine subduction zone during the late Eocene.

2.3 Exhumation models and implications on the deep orogenic structure

In general terms, exhumation models applied to (U)HP belts can be framed within two different groups, also implying alternative scenarios of mantle involvement: (i) synconvergent exhumation models, either requiring fast erosion or forced circulation in a low-viscosity wedge (e.g., Beaumont et al., 2001; Zeitler et al., 2001; Jamieson and Beaumont, 2013), and (ii) exhumation models that consider boundary divergence within the subduction zone, with a minor role played by erosion (e.g., Dewey, 1980; Brun and Faccenna, 2008). Both categories of models have been applied to the Western Alps (e.g., Malusà et al., 2011; Butler et al., 2013).

Classic tectonic reconstructions of the Alpine belt suggest that synconvergent exhumation could be favoured by deep duplex formation via the accretion of continental material derived from the lower plate (Schmid et al., 2004; Agard et al., 2009), which may be followed by indentation of the upper-plate mantle beneath the accretionary wedge (Schmid and Kissling, 2000; Béthoux et al., 2007). This scenario would imply that seismic velocities in the upper-plate mantle should be similar beneath the orogenic wedge and in the hinterland (Fig. 2B). In case of divergent motion between the upper plate and the descending slab, (U)HP rock exhumation might be instead associated to the emplacement of serpentinized mantle-wedge rocks at shallow depth beneath (U)HP continental rocks, provided that divergence is sufficiently high (Fig. 2C). Because of widespread mantle-wedge serpentinization during subduction (Lafay et al., 2013; Plümper et al., 2017), seismic velocities are predicted to be lower in mantle-wedge rocks beneath the (U)HP dome, and higher in adjoining dry mantle rocks of the upper plate (Fig. 2C).

These alternative scenarios would be in agreement with alternative end-member tectonic reconstructions of the southern Western Alps, based on recent geophysical data from the CIFALPS experiment (Zhao et al., 2016b). One possible end-member reconstruction, consistent with geophysical data, invokes a thick complex of (U)HP continental slivers, in line with predictions of numerical models of syn-convergent exhumation, whereas a second end-member reconstruction invokes a larger volume of mantle rocks possibly exhumed at shallow depth during divergent

motion within the subduction zone (Zhao et al., 2015; Malusà et al., 2017). A local earthquake tomography model, complementing previous studies based on receiver function analysis, would be extremely useful to discriminate between these end-member tectonic reconstructions, and may allow a decisive step forward in our understanding of mechanisms leading to exhumation of (U)HP rocks.

3. Methods

3.1. Building the database

The local earthquake tomography presented in this work is largely based on the dataset collected during the CIFALPS experiment (Zhao et al., 2016b), which was integrated by data recorded in the same time interval by permanent seismic networks operating in Italy and France, and complemented with selected older events. The temporary network of the CIFALPS experiment (blue marks in Figure 1B) includes 46 broadband seismic stations deployed along a linear WSW-ESE transect from the European foreland to the western Po Plain, and 9 additional stations installed to the north and to the south of the main profile. Stations operated from July 2012 to September 2013, and were specifically deployed for a direct comparison between receiver function and local earthquake tomography. Stations located along the main profile were conceived for receiver function analysis (Zhao et al., 2015). Their spacing ranges from ~5 km in the Western Alps mountain range to ~10 km in the European foreland and in the western Po Plain. Off profile stations were installed to improve the crossing of seismic rays for local earthquake tomography.

The high number of recording stations along the main CIFALPS profile may increase the computational burden during local earthquake tomography (e.g. in ray tracing) without a direct improvement in the final resolution. However, it ensures a number of advantages. For example, any potential loss of data due to station malfunctioning is easily recovered by adjacent instruments, and doubtful data can be discarded without jeopardizing the quality of the dataset. In order to improve the ray coverage and ensure ray crossing from any azimuth in the study volume, we added to the

dataset all published phase pickings recorded by permanent seismic stations operating in France and Italy during the CIFALPS experiment (red marks in Figure 1B). We additionally considered few events that occurred before the experiment to fill specific spatial gaps. This was the case of the intermediate depth earthquakes that were useful to sample anomalies at the bottom of the study volume. Because these earthquakes are relatively rare (Eva et al., 2015), only few events were recorded during the CIFALPS experiment. In summary, 270 events on a total of 1088 events utilized in this work were added as supplementary entries from datasets available at French and Italian seismic networks; about 80% of the remaining events were merged with existing phase pickings. The final P and S ray coverage is shown in Figure 3A.

3.2. Seismic tomography setup and reconstruction test

We adopted the local earthquake tomography code SIMULPS (Thurber, 1983) for tomographic analysis, in its version 14 that implements the ray tracer by Virieux (1991) to cope with models of regional size. We subdivided the study volume into layers containing nodes, and used an initial velocity model derived from previous seismic experiments over a larger area (Scafidi et al., 2009). Several tests were performed for a correct choice of the inversion parameters, and classical damping trade-off curves (Eberhart-Phillips, 1986) were computed to pick up the best values for P and S velocities.

The resolution capability of the coupling between inversion setup and data was evaluated by checkerboard and reconstruction tests. These tests were useful to choose an adequate geometry of the starting model and evaluate the smearing due to the contrast between high and low velocity anomalies. The reconstruction test was specifically conceived to test the potential impact of the high-velocity Ivrea body, a long recognized tectonic feature associated to a positive gravimetric anomaly (red dotted line in Fig. 1) and interpreted as a slice of Adriatic mantle emplaced at shallow depth (Closs and Labrouste, 1963; Nicolas et al., 1990). We used a “stairwell” geometry to simulate a high-velocity east-dipping layer along the CIFALPS profile (Fig. 3B) and test the resolution

capability of the coupling between seismic dataset and inversion setup. The same geometry after interpolation by the algorithm used in SIMULPS is shown in Figure 3C. A comparison with Figure 3B shows that the interpolation process introduces a smoothing of the anomalies and a band of fake colors around them. Figure 3D shows the reconstruction of the imposed stairwell structure based on our seismic dataset. The inversion of synthetic data does not consider the resolution, and Figure 3D only displays the reconstructed model as if it was completely resolved except for areas that were not sampled (in white). As shown in the reconstruction test, the shape of the anomaly is well reproduced, but the velocity of the first and second steps is lowered from ~8.0 km/s (blueish) to about ~7.5 km/s (greenish), and weak vertical and horizontal periodic stripes of yellow color appear at ~50 km depth. These artifacts, and the undestimation of the magnitude of the high velocity anomalies in the uppermost 10 km of the crust, have been considered during the subsequent phases of tomography interpretation. The real data tomographic model is about 700×700 km wide, and was obtained after 6 iterations on a 12 layers model of 36×36 nodes each. In the central part of the model, spacing between nodes is equal to 15 km.

4. Results

Figure 4 shows the Vp and Vp/Vs cross-sections along the CIFALPS profile. The lighter areas are those where the diagonal elements of the resolution matrix are <0.1. This threshold was chosen as the divider between resolved and non-resolved areas based on a comprehensive comparisons between different resolution indicators (Paul et al., 2001). As expected, the maximum depth of the resolved area is limited by the depth of occurrence of most of the deepest events (Eva et al., 2015; Malusà et al., 2017). Beneath the Dora-Maira (U)HP dome, the tomography model is well resolved down to 50-60 km depth, whereas the two extremes of the CIFALPS cross section are poorly resolved. Letters “a” to “k” indicate the relevant velocity features highlighted by the tomography model. The main tectonic structures previously inferred from receiver function analysis (Zhao et al.

263 2015) and surface geology (Lardeaux et al., 2006; Malusà et al., 2015) are also indicated for
264 comparison (black lines in Fig. 4).

265 The most prominent feature of the tomography model is represented by the high velocity body
266 (Vp ~7.5 km/s; Vp/Vs = 1.70-1.72), labelled with "a", which is located right below the Dora-Maira
267 (U)HP dome, at depths as shallow as ~10 km. Such a high-velocity body was already imaged with
268 similar velocities by previous works (Vp ~7.4-7.7 km/s; Paul et al., 2001; Béthoux et al., 2007), but
269 was only resolved down to depths of 15-20 km. It is still observed to the south of the CIFALPS
270 profile (Fig. 5D,E), but progressively vanishing towards the north (Fig. 5A,B). A series of N-S
271 cross sections, ranging from the Western Alps to the Po Plain (Fig. 6), shows that this high-velocity
272 anomaly is exclusively found beneath the Dora-Maira (U)HP dome (Fig. 6A), and disappears
273 farther east.

274 The mantle-wedge region labelled with "b" is located at depth of 20-45 km, in correspondence
275 with a cluster of intermediate depth earthquakes that mark the Rivoli-Marene deep fault (RMF in
276 Fig. 4A; Eva et al., 2015). This region shows higher Vp values (~8.0 km/s) compared to region "a",
277 and anomalously high Vp/Vs ratios (>1.74) that are supportive of low shear wave velocities. This
278 cluster of intermediate depth earthquakes in region "b" is not only observed along the CIFALPS
279 profile, but also in cross sections located more to the north or to the south (Fig. 5). The deepest
280 mantle wedge region resolved by the tomographic model is labelled with "c". This region, located
281 at depth of ~40-50 km atop the European slab, shows lower Vp and Vp/Vs values compared to
282 region "b" (Vp ~7.0-7.5 km/s; Vp/Vs < 1.70), but the Vp/Vs ratio is locally higher (Vp/Vs ~1.74).

283 The well-resolved regions of the model also include some subducted European lower crust. This
284 shows a progressive increase in Vp from the region labelled with "d" (Vp ~6.7 km/s) to the region
285 labelled with "e" (Vp ~7.6 km/s), under a rather constant Vp/Vs ratio of 1.70-1.72. Such variations
286 are detected in all of the analyzed WSW-ENE transects of Figure 5. No seismic event was recorded
287 in regions "d" and "e" since 1990 (installation of permanent seismic networks) and during the
288 CIFALPS experiment (Malusà et al., 2017).

On the eastern side of the transect, the region labelled with “f” is located below the Adriatic Moho as determined by receiver function analysis combined with gravity modelling. It shows Vp values ~8.0 km/s and Vp/Vs = 1.70-1.72. This region is affected by intermediate depth earthquakes that are also observed to the north and to the south of the CIFALPS transect (Fig. 5). The vertical and horizontal periodic stripes of yellow color observed at 50 km depth in this region are artifacts, as confirmed by the reconstruction test of Fig. 3D. Above the Adriatic Moho, measured Vp values are much lower, generally <6.7 km/s, but in places they reach values as high as ~7.2 km/s. Very high Vp/Vs values (>1.8) are locally observed at ~30 km depth at the base of the Adriatic crust. This region, labelled with “g”, is also characterized by a cluster of seismic events that are only observed in the vicinity of the main CIFALPS transect.

In the uppermost part of the Alpine orogenic wedge (regions “h” to “k”), Vp values are invariably <6.5 km/s, but major variations in Vp/Vs ratios are locally observed. For example, the region to the east of the Dora-Maira (U)HP dome (labelled with “h”) shows Vp/Vs values >1.72, whereas the region corresponding to the western flank of the Dora-Maira dome (labelled with “j”) shows much lower Vp/Vs ratios, even <1.66. Vp/Vs ratios <1.68 are also observed in the region labelled with “k”, located beneath the Frontal Pennine Fault. The double-vergence accretionary wedge located to the east of the Frontal Pennine Fault, and labelled with “i”, shows instead Vp/Vs values > 1.75, and includes most of the shallow earthquakes recorded in the Western Alps area.

5. Comparison with receiver function analysis

Results of local earthquake tomography are compared in Figure 7 with published CIFALPS results of receiver function analysis (Zhao et al., 2015). Unlike local earthquake tomography, the receiver function technique is based on the analysis of teleseismic earthquakes, and enhances P-to-S (Ps)-converted waves on velocity interfaces beneath an array. The polarity of the converted signal depends on the sign of the velocity change, and interfaces with velocity increase can be discriminated from interfaces with velocity decrease. Assumptions and arbitrary choices of the

receiver function approach applied to the CIFALPS transect (e.g., magnitude threshold, epicentral distance, seismograms filtering, velocity model, choice of the direction of back azimuths) are described in full in Zhao et al. (2015).

The image of Figure 7B is based on radial receiver functions from teleseismic events with magnitude ≥5.5, epicentral distance of 30-90°, and ENE back-azimuths (see Zhao et al., 2015). This image shows two major interfaces marked by positive-polarity Ps-conversions (red-to-yellow regions), which attest the downward velocity increase corresponding to the European and Adriatic Mohos (thick dashed lines). The eastward-dipping European Moho is recognized from ~40 km depth beneath the Frontal Pennine Fault to ~75 km depth beneath the Po Plain. The Adriatic Moho is recognized from 20-30 km depth, to the east, to 10-15 km depth, to the west. The red spots located at 40-55 km depth beneath the Adriatic Moho are multiples, as confirmed by synthetic tests (Zhao et al., 2015). A shallow positive-polarity converted phase is also observed beneath the Dora-Maira massif, between regions "a" and "h", whereas a spot of negative-polarity Ps-conversions marking a downward velocity decrease is located above region "c", at 20-40 km depth (blue region).

On the eastern side of the CIFALPS transect, the sharp velocity increase from Vp <6.5 km/s to Vp >8 km/s evidenced by local earthquake tomography faithfully matches the location of the downward velocity increase highlighted by receiver function analysis. Localized anomalies in Vp/Vs ratios, e.g., in region "g", match with major breaks in the alignment of positive-polarity Ps-conversions. Beneath the Dora-Maira (U)HP dome, the downward increase in Vp values from region "h" (Vp <6.5 km/s) to region "a" (Vp ~7.5 km/s) is consistent with the observed positive-polarity Ps-conversions, whereas the downward velocity decrease from regions "a" and "b" (Vp ~7.5 km/s and >8 km/s) to region "c" (Vp ~7.0-7.5 km/s) is consistent with the spot of negative-polarity Ps-conversions located at 20-40 km depth in Figure 7B. The shape of the high-velocity region labelled with "a" is also mirrored by the distribution of seismic events recorded since 1990. Region "a" is virtually aseismic (Malusà et al., 2017), and earthquakes are chiefly located along its

external boundaries or in the surrounding regions (Fig. 7B). On the western side of the CIFALPS transect, the alignment of positive-polarity Ps-conversions generated along the European Moho is partly included within the resolved area of the local earthquake tomography model, and fits with a downward velocity increase from ~6.7 km/s (region "d") to ~7.6 km/s (region "e"). The velocity structure unravelled by the analysis of local earthquakes is thus independently confirmed by the analysis of teleseismic earthquakes (Zhao et al., 2015) and by the distribution of seismic events (Eva et al., 2015; Malusà et al., 2017).

6. Geologic interpretation

The geologic cross section of Figure 7C shows the main features of the orogenic wedge of the Western Alps, and of the mantle wedge between the European and the Adriatic plates, as inferred from the velocity structure derived from local earthquake tomography along the CIFALPS profile. Correlation between seismic velocity and lithology in former subduction zones is a challenging task. Subducted rocks are heterogenous, and display anisotropic fabrics and velocity variations as a function of direction (e.g., Rudnick and Fountain, 1995; Weiss et al., 1999). A full 3D coverage of seismic rays is thus required to get a reliable characterization of the velocity structure (see Fig. 3A).

In the European plate, the Vp values ~6.7 km in region "d" are supportive of a relatively felsic composition of the European lower crust (e.g. Rudnick and Fountain 1995; Weiss et al., 1999; Goffé et al. 2003; Wang et al., 2005; Mechie et al. 2012). The homogeneous Vs values < 4 km/s reported by Lyu et al. (2017) suggest that the European lower crust may be rather homogeneous at the scale of seismic observations, and may consist of granulite having felsic to intermediate composition. Major occurrence of granulitic metapelites can be safely excluded, because it would result in much higher Vp (>6.7 km/s up to 7.2 km/s) and Vs values (~4 km/s; Rudnick and Fountain, 1995).

The increase in Vp values evidenced at ~40 km depth by local earthquake tomography, from ~6.7 km/s in region "d" to ~7.6 km/s in region "e", may mirror a progressive eclogitization of lower

crust rocks with consequent density increase by metamorphic phase changes (e.g., Hacker et al., 2003; De Paoli et al., 2012). Mineral equilibria at the granulite-eclogite transition depend on rock composition. The eclogitization of a felsic granulite strongly increases the garnet content, and consequently the density from 2.90 to 3.30 kg/dm^3, and the P velocity up to a maximum of 7.6 km/s (e.g., Christensen, 1989; Hacker et al., 2003, 2015; Hacker and Abers, 2004; Hetényi et al., 2007). These values are consistent with the Vp values observed in region "e". The increase in P velocity from region "d" to region "e" is associated with a progressive increase in S velocity up to 4.2 km/s (Lyu et al., 2017), which may be either interpreted as an increase in mafic component, or as an effect of metamorphic reactions under increasing pressure-temperature conditions. However, Vp values in region "e" are far too low for a pure mafic eclogite (Bezacier et al., 2010; Reynard, 2013), thus suggesting no major compositional changes from west to east in the European lower crust, but only a progressive change in metamorphic assemblage during subduction. This interpretation also explains the progressive weakening of the positive-polarity converted phases observed along the European Moho, from red to yellow background colours in Fig. 7B, as previously described by Zhao et al. (2015).

On the eastern side of the Western Alps, Vp values >8 km/s confirm the presence of Adriatic mantle at shallow depth beneath the western Po Plain (10-15 km), just in correspondence with the positive gravimetric anomaly classically referred to as the Ivrea body (Closs and Labrouste, 1963; Nicolas et al., 1990) and in line with results of previous tomographic models (e.g., Solarino et al., 1997; Paul et al., 2001; Scafidi et al., 2006; 2009; Diehl et al., 2009; Wagner et al., 2012). East of the Ivrea body gravimetric anomaly, the Adriatic Moho is located at 30-35 km depth, which is a much more reliable estimate of the Moho depth beneath the Po Plain compared to previous estimates based on receiver function alone (Zhao et al., 2015). The locally high Vp/Vs ratios >1.8, associated to Vp of 7.0-7.5 km/s (region "g"), may be supportive of gabbro (Weiss et al., 1999) underplated at the base of the Adriatic lower crust. Noteworthy, Permian gabbros are indeed exposed north of the Po plain, where they are intruded into lower crust rocks belonging to the

391 Adriatic (Southalpine) basement (Quick et al., 1994; Schaltegger and Brack, 2007). Above the
392 Adriatic Moho, local spots with Vp ~7.2 km/s but low Vp/Vs ratios (Fig. 5) are supportive of a
393 more heterogeneous composition of the Adriatic lower crust compared to the European lower crust,
394 and may suggest a local occurrence of granulite facies metapelites (Vp 6.7-7.2 km/s, Vs ~4 km/s;
395 Rudnick and Fountains, 1995) not only at the surface (e.g., Ewing et al., 2014), but also at depth.
396 Differences in velocity structure among crustal sections now exposed on the opposite sides of the
397 Alps probably reflect a different pre-Alpine evolution, rather than processes related to the Cenozoic
398 evolution of the Adria-Europe plate boundary zone (Guillot et al., 2009b; Carosi et al., 2012;
399 Bergomi et al., in review).
400 In the uppermost part of the Alpine wedge, the structural variability of stacked rocks is largely
401 mirrored by their variability in Vp/Vs ratios. The Vp/Vs values >1.75 observed in the double-
402 vergence accretionary wedge chiefly including Briançonnais and Schistes lustrés units (Lardeaux et
403 al., 2006), may reflect low Vs values, possibly associated to the widespread network of mesoscale
404 faults developed in these rocks since the Neogene (Tricart et al., 2004; Sue et al., 2007; Malusà et
405 al., 2009). To the east, low Vp/Vs values even <1.66 observed on the western flank of the Dora-
406 Maira dome (region "j") may instead reflect high Vs velocities, suggesting that the poorly fractured
407 granitic gneisses exposed at the surface (Brossasco granite; Paquette et al., 1999; Lenze and
408 Stöckhert, 2007) may be also present at depth. Fracturing may be also invoked to explain the low
409 Vs values observed along the eastern boundary of the Dora-Maira dome, where (U)HP continental
410 rocks are juxtaposed against the eclogitized mantle rocks of the Lanzo massif (Kienast and
411 Pognante, 1988; Piccardo et al., 2007) along the Lis-Trana deformation zone (Perrone et al., 2010).
412 To the west of the Frontal Pennine Fault, Vp/Vs values <1.68 suggest instead that the European
413 upper crust in the External zones is poorly deformed, consistent with minor seismicity recorded in
414 that area (Fig. 7B).
415 But the most relevant results of the tomography model presented in this work is related to the
416 velocity structure beneath the Dora-Maira (U)HP dome. This information is critical to discriminate

between contrasting models of (U)HP rock exhumation (Malusà et al., 2011, 2015; Jamieson and Beaumont, 2013), and to discern between end-member tectonic reconstructions recently proposed in the light of available geophysical data (Malusà et al., 2017). The velocity structure of the mantle wedge region "a", showing Vp velocity of ~7.5 km/s from depths as shallow as ~10 km down to ~30 km, is largely inconsistent with the presence of imbricated continental crust units (e.g., Schmid et al., 2017) or dry mantle peridotite beneath the Dora-Maira (U)HP dome. Instead, it may suggest a complex evolution of mantle-wedge rocks in terms of P-T conditions and fluid-rock interaction. Such Vp values point in fact to widespread serpentinization of mantle rocks (~60% according to Reynard, 2013), that may locally exceed 90% both in the uppermost part of anomaly "a" and in the Lanzo massif, although velocity values in the uppermost crustal levels may be slightly underestimated, as unravelled by the reconstruction tests of Fig. 3D. The degree of serpentinization at 30-40 km depth is instead much lower (<30%), and consistent with the occurrence of intermediate-depth earthquakes (Fig. 7B). Vp/Vs ratios are in the range of 1.70-1.72 in region "a", but sharply increase to values >1.74 in region "b", where Vp values (~8.0 km/s) are consistent with dry mantle peridotite. The high Vp/Vs ratios in region "b" point to low shear wave velocities, which are in line with a potential impact of the Rivoli-Marene deep fault on the rock fabric. According to previous work, the deepest part of the mantle wedge beneath the thick blue spot of negative polarity conversions (region "c" in Fig. 7B) may either include serpentinites, or slivers of (U)HP rocks. On a geophysical ground, serpentinites can be easily distinguished from other lithologies possibly found in high-pressure mélange zones (e.g., Marschall and Schumacher, 2012) such as eclogitic metasediments and mafic eclogites (Reynard, 2013). Our results indicate that the velocity values observed in region "c" (Vp ~7.0-7.5 km/s; Vp/Vs <1.70) are neither consistent with eclogitic metasediments (Vp ~7.0 km/s; Vp/Vs ~1.75) nor with mafic eclogite (Vp > 8.0 Vp/Vs ~1,73), but are instead supportive of ultramafic rocks with a degree of serpentinization ranging between 50% and 75% (Weiss et al., 1999; Reynard, 2013). However, minor slivers of eclogitic metasediments

could be present at ~40 km depth at the top of the European slab, in regions showing the highest Vp/Vs ratios (Fig. 7A).

7. Implication for (U)HP rock exhumation

In the southern Western Alps, the positive gravimetric anomaly ascribed to the Ivrea body is classically interpreted in terms of upper mantle indentation (e.g., Lardeaux et al., 2006; Béthoux et al., 2007), in line with previous tectonic interpretations proposed for the Central Alps and for the northern Western Alps (e.g., Schmid and Kissling, 2000). According to these interpretations, the uppermost part of the Adriatic mantle would act as an indenter beneath the Alpine accretionary wedge, and would transfer compression towards the European foreland. The main geologic implications of this model include major crustal shortening in the upper plate, and fast erosion focused above the indenter (Fig. 2B). These latter features are indeed observed in the Central Alps, where upper mantle indentation, accommodated by back-folding of (U)HP domes (Keller et al., 2005) and by backthrusting of Adriatic units (Zanchetta et al., 2015), triggered the fast erosional exhumation of the amphibolite-facies rocks of the Lepontine dome (Anfinson et al., 2016; Malusà et al., 2016b). However, these features are not common to the southern Western Alps, where shortening in the accretionary wedge was minor during and after (U)HP rock exhumation (Malusà et al., 2009; Dumont et al., 2012), and erosion was much slower compared to the Lepontine dome, as attested by low-temperature thermochronometers (Malusà et al., 2005b; Vernon et al., 2008; Fox et al., 2015) and by preserved Oligocene corals unconformably lying on top of Eocene eclogites (Molare Fm; Quaranta et al. 2009). A tectonic scenario exclusively invoking upper-plate mantle indentation beneath the accretionary wedge would also imply that seismic velocities in the upper-plate mantle should be quite similar beneath the orogenic wedge and in the hinterland (Fig. 2B). Major seismic velocity changes, e.g., by metamorphic phase changes triggered by fluids released by the downgoing slab, would remain undetected in local earthquake tomography models, because they would take place at much greater depths (Deschamps et al., 2013; Abers et al., 2017).

Our study points to a complex velocity structure in the upper-plate mantle of the southern Western Alps. The region beneath the Dora-Maira (U)HP dome is dominated by serpentinized peridotites, documented from ~10 km depth down to the top of the European slab. To the east, these rocks are juxtaposed against dry mantle peridotites of the Adriatic upper plate along a steeply dipping fault rooted in the lithospheric mantle (RMF in Fig. 7C). In between, mantle rocks of the Lanzo massif underwent subduction during the Alpine orogeny, and were later exhumed and accreted against the Adriatic upper plate when the Dora-Maira (U)HP rocks were still buried at mantle depths (Rubatto and Hermann, 2001). This scenario is supportive of (U)HP rock and mantle-wedge exhumation triggered by upper plate divergent motion (Fig. 2C).

Serpentinized peridotites with Vp ~7.5 km/s that are found beneath the Dora-Maira dome may have favoured the exhumation of (U)HP rocks across the upper crust, in the depth range where eclogitized continental crust rocks may have become neutrally buoyant (Schwartz et al., 2001). According to Agard et al. (2009), exhumation of eclogitized ophiolites woud be favoured by accretion of continental material. Our results point instead to a decisive role played by buoyant serpentinites (e.g., Hermann et al., 2000; Schwartz et al., 2001) during continental (U)HP rock exhumation, within a broadly extensional tectonic framework that is common to many recent tectonic reconstructions of the Central Mediterranean area (e.g., Vignaroli et al., 2008; Malusà et al., 2015) (Fig. 8).

No exhumed mantle-wedge serpentinites are recognized so far at outcrop in the southern Western Alps (Scambelluri et al., 1995; Piccardo et al., 2004; Hattori and Guillot, 2007; Deschamps et al., 2013). However strong fluid-rock interactions are recognized in subducted serpentinites and associated ophiolitic rocks (Scambelluri and Tonarini, 2012; Lafay et al., 2013; Plümper et al., 2017), suggesting that fluid release may have occurred during oceanic and even during continental subduction (e.g., Castelli et al., 2007; Ferrando et al., 2009), possibly triggering the partial serpentinization of the Adriatic mantle wedge. Part of the Adriatic mantle wedge was then exhumed at shallow crustal levels during late Eocene transtension along the Western Alps subduction zone

493 (Malusà et al., 2015) and coeval rapid exhumation of the Dora-Maira (U)HP rocks (Rubatto and
494 Hermann, 2001) (step 1 in Fig. 8). The exhumed mantle wedge was finally indented beneath the
495 Alpine belt during early Oligocene tectonic shortening (Dumont et al., 2012; Jourdan et al., 2012,
496 2013) (step 2 in Fig. 8). Along the Adria-Europe plate boundary, the divergent component of
497 Eocene transtension progressively decreased towards the north to become negligible in the Central
498 Alps (Fig. 8A), where Adria was indented more deeply beneath the accretionary wedge compared to
499 the Western Alps, and rocks now exposed in the Lepontine dome were exhumed at lower rates
500 through the upper crust (Fig. 8B). We speculate that, north of the Dora-Maira dome, upper plate
501 divergence was probably insufficient to allow an effective exhumation of the mantle wedge (Fig.
502 8C). However, testing this hypothesis would require a high resolution tomographic image of the
503 northern Western Alps, which may be precluded by the lack of deep earthquakes.

504 Our results demonstrate that recent geologic cross-sections postulating a thick wedge of
505 Briançonnais eclogites beneath the Dora-Maira dome (e.g., Schmid et al., 2017) are likely incorrect.
506 The palinspastic reconstructions derived from such geologic cross-sections, and exclusively
507 considering a Cenozoic evolution within a broadly compressional framework, should be
508 reconsidered at the advantage of palinspastic reconstructions also including major episodes of
509 divergence within the plate boundary zone (e.g., Vignaroli et al., 2008; Malusà et al., 2015). Mantle
510 wedge exhumation is in fact more consistent with a late Eocene transtensional tectonic framework
511 (Fig. 8C) followed by early Oligocene convergence (Fig. 8D), accommodated by orogen-
512 perpendicular shortening in the external Alps (Dumont et al., 2012) and by transpressional tectonics
513 in the Alps-Apennines transition zone (Malusà and Balestrieri, 2012).

514 The occurrence of mantle-wedge serpentinites exhumed at shallow depth within a continental
515 subduction zone is not specific of the southern Western Alps. Mantle wedge serpentinites associated
516 with (U)HP rock are described, for example, in the Indus Suture Zone in the Himalaya, in the
517 Carribbean (Guillot et al., 2001; Deschamps et al., 2012), in the Western Gneiss Region in Norway
518 (Scambelluri et al., 2010), and are inferred by geophysical evidence under the Dabie-Sulu (Liu et

519 al., 2015). Our findings suggest that orogen-scale exhumation of the mantle wedge may represent a
520 prominent, but still underestimated feature of the deep structure of many orogenic belts. As such, it
521 should be integrated in more advanced theoretical models of subduction and exhumation. Moreover,
522 widespread mantle-wedge exhumation may explain the common occurrence of boudinaged mantle-
523 wedge rocks within continental UHP rocks in the roots of old orogenic belts now unroofed by
524 erosion. In pre-Cenozoic orogenic belts such as the Dabie-Sulu or the Western Gneiss Region,
525 where the evidence of minor erosion during UHP exhumation, if any, is no longer preserved, the
526 occurrence of mantle wedge rocks at shallow depth may represent the only evidence supporting
527 (U)HP rock exhumation triggered by divergent motion between upper plate and accretionary
528 wedge.

529 **8. Conclusions**

530 The new local earthquake tomography model of the southern Western Alps, independently
531 validated by receiver function analysis, unravels a complex seismic velocity pattern consistent with
532 a composite structure of the mantle wedge above the subducted European lithosphere. Seismic
533 velocities indicate that the Dora-Maira (U)HP dome lays directly above serpentinized peridotites,
534 documented from ~10 km depth down to the top of the eclogitized lower crust of the European
535 plate. We propose that peridotite serpentinization was the result of fluids released to the Adriatic
536 mantle wedge during Alpine subduction. During late Eocene transtension, when the subduction
537 wedge was largely exhumed at the Earth's surface, part of the mantle wedge was also exhumed at
538 shallow crustal levels, to be finally indented under the Alpine metamorphic units in the early
539 Oligocene. Our results suggest that mantle wedge exhumation may represent an important feature of
540 the deep structure of exhumed continental subduction zones. Deep orogenic levels, as those imaged
541 by local earthquake tomography in the southern Western Alps, may be exposed today in older
542 continental subduction zones, where mantle wedge serpentinites are commonly associated to
543 continental (U)HP metamorphic rocks.

Acknowledgments. This work is funded by the State Key Laboratory of Lithospheric Evolution, China, the National Natural Science Foundation of China (Grant 41350001), and a grant from LabEx OSUG@2020 (Investissements d'avenir; ANR10 LABX56, France). The earthquake waveforms used in this study are available at the European Integrated Data Archive (eida.rm.ingv.it) (see also doi:10.13127/SD/X0FXnH7QfY; doi:10.12686/sed/networks/2a). The CIFALPS seismic data are archived at the data center of the Seismic Array Laboratory, Institute of Geology and Geophysics, Chinese Academy of Sciences, and at the data center of the French Seismologic and Geodetic Network RESIF (doi:10.15778/RESIF.YP2012). The manuscript benefited from constructive reviews by F. Rossetti and an anonymous reviewer, comments by M. Scambelluri, and insightful discussions with S. Baldwin, S. Ferrando and N. Malaspina.

References

Abers, G. A., van Keken, P. E., Hacker, B. R., 2017. The cold and relatively dry nature of mantle forearcs in subduction zones. Nature Geoscience 10(5), 333-337.

Agard, P., Monie, P., Jolivet, L., Goffé, B., 2002. Exhumation of the Schistes Lustrés complex: In situ laser probe Ar-40/Ar-39 constraints and implications for the western Alps. Journal of Metamorphic Geology 20, 599–618.

Agard, P., Yamato, P., Jolivet, L., Burov, E., 2009. Exhumation of oceanic blueschists and eclogites in subduction zones: timing and mechanisms. Earth-Science Reviews 92(1), 53-79.

Angiboust, S., Langdon, R., Agard, P., Waters, D. J., Chopin, C. 2012. Eclogitization of the Monviso ophiolite (W Alps) and implications on subduction dynamics. Journal of Metamorphic Geology 30, 37–61.

Avigad, D., Chopin, C., Le Bayon, R., 2003. Thrusting and extension in the southern Dora-Maira ultra-high-pressure massif (Western Alps): view from below the coesite-bearing unit. The Journal of geology 111(1), 57-70.

Ballèvre, M., Lagabrielle, Y., Merle, O., 1990. Tertiary ductile normal faulting as a consequence of lithospheric stacking in the western Alps. Société Géologique de France, Mémoires 156, 227–236.

Beaumont, C., Jamieson, R.A., Nguyen, M.H., Lee, B., 2001. Himalayan tectonics explained by extrusion of a low-viscosity crustal channel coupled to focused surface denudation. Nature 414, 738-742.

Becker, H., 1993. Garnet peridotite and eclogite Sm-Nd mineral ages from the Lepontine dome (Swiss Alps): New evidence for Eocene high-pressure metamorphism in the central Alps. Geology 21, 599-602.

Beltrando, M., Compagnoni, R., Lombardo, B., 2010. (Ultra-) High-pressure metamorphism and orogenesis: An Alpine perspective. Gondwana Research 18(1), 147-166.

Bergomi, M.A., Dal Piaz, G.V., Malusà M.G., Monopoli, B., Tunesi, A. The Grand St Bernard - Briançonnais nappe system and the Paleozoic inheritance of the Western Alps unravelled by zircon U-Pb dating. Tectonics (in review).

Béthoux, N., Sue, C., Paul, A., Virieux, J., Fréchet, J., Thouvenot, F., Cattaneo, M., 2007. Local tomography and focal mechanisms in the south-western Alps: comparison of methods and tectonic implications. Tectonophysics 432, 1–19.

Beucher, R., van der Beek, P., Braun, J., Batt, G. E., 2012. Exhumation and relief development in the Pelvoux and Dora-Maira massifs (western Alps) assessed by spectral analysis and inversion of thermochronological age transects. Journal of Geophysical Research: Earth Surface, 117(F3).

583 Bezacier, L., Reynard, B., Bass, J.D., Wang, J., Mainprice, D., 2010. Elasticity of glaucophane, seismic
584 velocities and anisotropy of the subducted oceanic crust. Tectonophysics 494, 201–210.

585 Blake, M.C., Jayko, A.S., 1990. Uplift of very high pressure rocks in the western Alps: Evidence for
586 structural attenuation along low angle faults. In: Roure, F., Heitzmann, P., Polino, R. (Eds.), Deep
587 structure of the Alps. Mémoire de la Société Géologique de France 156, pp. 228–237.

588 Boudier, F., 1978. Structure and petrology of the Lanzo peridotite massif (Piedmont Alps). Geological
589 Society of America Bulletin 89(10), 1574-1591.

590 Brouwer, F.M., van de Zedde, D.M.A., Wortel, M.J.R., Vissers, R.L.M, 2004. Late-orogenic heating during
591 exhumation: Alpine PTt trajectories and thermomechanical models. Earth and Planetary Science
592 Letters 220, 185-199.

593 Brun, J. P., Faccenna, C., 2008. Exhumation of high-pressure rocks driven by slab rollback. Earth and
594 Planetary Science Letters 272(1), 1-7.

595 Butler, J.P., Beaumont, C., Jamieson, R.A., 2013. The Alps 1: A working geodynamic model for burial and
596 exhumation of (ultra) high-pressure rocks in Alpine-type orogens. Earth and Planetary Science Letters
597 377, 114–131.

598 Carosi, R., Montomoli, C., Tiepolo, M., Frassi, C., 2012. Geochronological constraints on post-collisional
599 shear zones in the Variscides of Sardinia (Italy). Terra Nova 24(1), 42-51.

600 Carswell, D. A., R. Compagnoni (Eds.), 2003. Ultrahigh Pressure Metamorphism, 508 pp., Eotvos Univ.
601 Press, Budapest.

602 Castelli, D., Rolfo, F., Groppo, C., Compagnoni, R., 2007. Impure marbles from the UHP Brossasco-Isasca
603 Unit (Dora-Maira Massif, western Alps): evidence for Alpine equilibration in the diamond stability
604 field and evaluation of the X(CO_2) fluid evolution Journal of Metamorphic Geology, 25, 587-603

605 Chen, Y. X., Zhou, K., Zheng, Y. F., Schertl, H. P., 2017. Zircon geochemical constraints on the protolith
606 nature and metasomatic process of the Mg-rich whiteschist from the Western Alps. Chemical Geology
607 467, 177-195.

608 Chopin, C., 1984. Coesite and pure pyrope in high-grade blueschists of the Western Alps: A first record and
609 some consequences. Contributions to Mineralogy and Petrology 86, 107–118.

610 Chopin, C., Henry, C., Michard, A., 1991. Geology and petrology of the coesite bearing terrain, Dora-Maira
611 massif, western Alps. European Journal of Mineralogy 3, 263–291.

612 Christensen, N.I., 1989. Seismic velocities. In: Carmichael, R.S. (Ed.), Practical Handbook of Physical
613 Properties of Rocks and Minerals. CRC Press, Boca Raton, p. 741.

614 Closs, H. and Labrouste Y. (Eds.), 1963. Rechèrches séismologiques dans les Alpes occidentales au moyen
615 de grandes explosions en 1956, 1958 et 1960. Mem. Coll. Année Geophys. Int. 12-2. CNRS Paris, 241
616 pp.

617 Compagnoni, R., Hirajima, T., Chopin, C., 1995. Ultra-high-pressure metamorphic rocks in the Western
618 Alps. In: Coleman, R.G., Wang, X. (Eds.), Ultrahigh Pressure Metamorphism. Cambridge University
619 Press, Cambridge, UK, pp. 206–243.

620 Compagnoni, R., Rolfo, F., 2003. UHPM units in the western Alps: European Mineralogy Union Notes in
621 Mineralogy 5, 13–49.

622 Coward, M., Dietrich, D., 1989. Alpine tectonics: an overview. In: Coward, M., Dietrich, D., Park, R.G.
623 (Eds), Alpine Tectonics. Geological Society, London, Special Publications 45, pp. 1–29.

624 De Paoli, M. C., Clarke, G. L., Daczko, N. R., 2012. Mineral equilibria modeling of the granulite–eclogite
625 transition: effects of whole-rock composition on metamorphic facies type-assemblages. Journal of
626 Petrology 53(5), 949-970.

627 Debret, B., Nicollet, C., Andreani, M, Schwartz, S., Godard, M., 2013. Three steps of serpentinization in an
628 eclogitised oceanic serpentinisation front (Lanzo massif - Western Alps). Journal of Metamorphic
629 Geology 31, 165–186.

630 Deschamps, F., Godard, M., Guillot, S., Chauvel, C., Andreani, M., Hattori K., Wunder B., France L., 2012.
631 Behavior of fluid-mobile elements in serpentines from abyssal to subduction environments: Examples
632 from Cuba and Dominican Republic. Chemical Geology 313, 93–117.

633 Deschamps, F., Godard, M., Guillot, S., Hattori, K.H., 2013. Geochemistry of subduction zone serpentinites:
634 A review. Lithos 178, 96-127.

635 Dewey, J.F., 1980. Episodicity, sequence and style at convergent plate boundaries. Geological Association
636 of Canada Special Paper 2, 553-576.

637 Dewey, J. F., Helman, M. L., Knott, S. D., Turco, E., Hutton, D. H. W. (1989). Kinematics of the western
638 Mediterranean. Geological Society, London, Special Publications 45(1), 265-283.

639 Diehl, T., Husen, S., Kissling, E., Deichmann, N., 2009. High-resolution 3-D P-wave model of the Alpine
640 crust. Geophysical Journal International 179(2), 1133–1147.

641 Ducea, M. N., 2016. Research Focus: Understanding continental subduction: A work in progress. Geology
642 44, 239-240.

643 Duchêne, S., Blichert-Toft, J., Luais, B., Télouk, P., Lardeaux, J.M., and Albarède, F., 1997. The Lu-Hf
644 dating of garnets and the ages of the Alpine high-pressure metamorphism. Nature 387, 586–589.

645 Dumont, T., Schwartz, S., Guillot, S., Simon-Labric, T., Tricart, P., Jourdan, S., 2012. Structural and sedimentary
646 records of the Oligocene revolution in the Western Alps. Journal of Geodynamics 56, 18–38.

647 Eberhart-Phillips, D., 1986. Three-dimensional velocity structure in northern California Coast Ranges from
648 inversion of local earthquake arrival times. Bulletin of the Seismological Society of America 76(4),
649 1025–1052.

650 Eva, E., Malusà, M.G., Solarino, S., 2015. A seismotectonic picture of the inner southern Western Alps
651 based on the analysis of anomalously deep earthquakes. Tectonophysics 661, 190–199.

652 Ewing, T. A., Rubatto, D., Hermann, J., 2014. Hafnium isotopes and Zr/Hf of rutile and zircon from lower
653 crustal metapelites (Ivrea–Verbano Zone, Italy): implications for chemical differentiation of the crust.
654 Earth and Planetary Science Letters 389, 106-118.

655 Ferrando, S., Frezzotti, M. L., Petrelli, M., Compagnoni, R., 2009. Metasomatism of continental crust during
656 subduction: the UHP whiteschists from the Southern Dora-Maira Massif (Italian Western Alps).
657 Journal of Metamorphic Geology 27(9), 739-756.

658 Ferrando, S., Groppo, C., Frezzotti, M. L., Castelli, D., Proyer, A., 2017. Dissolving dolomite in a stable
659 UHP mineral assemblage: Evidence from Cal-Dol marbles of the Dora-Maira Massif (Italian Western
660 Alps). American Mineralogist 102(1), 42-60.

661 Ford, M., Duchêne, S., Gasquet, D., Vanderhaeghe, O., 2006. Two-phase orogenic convergence in the
662 external and internal SW Alps. Journal of the Geological Society 163, 815–826.

663 Fox, M., Herman, F., Kissling, E., Willett, S.D., 2015, Rapid exhumation in the Western Alps driven by slab
664 detachment and glacial erosion. Geology, 43, 379–382.

665 Ganne, J., Bertrand, J.M., Fudral, S., Marquer, D., Vidal, O., 2007. Structural and metamorphic evolution of
666 the Ambin massif (western Alps): toward a new alternative exhumation model for the Briançonnais
667 domain. Bulletin de la Société Géologique de France 178, 437–458.

668 Gebauer, D., 1996. A P-T-t path for an (ultra?-) high-pressure ultramafic/mafic rock-association and its felsic
669 country-rocks based on SHRIMP-dating of magmatic and metamorphic zircon domains. Example:
670 Alpe Arami (Central Swiss Alps), in: Basu, A., Hart, S. (Eds.), Earth Processes: Reading the Isotopic
671 Code. Geophys. Monograph 95, Am. Geophys. Union, Washington, DC, pp. 307-330.

672 Gebauer, D. H. P. S., Schertl, H. P., Brix, M., Schreyer, W., 1997. 35 Ma old ultrahigh-pressure
673 metamorphism and evidence for very rapid exhumation in the Dora Maira Massif, Western Alps.
674 Lithos 41, 5-24.

675 Gilotti, J. A., 2013. The realm of ultrahigh-pressure metamorphism. Elements 9, 255–260.

676 Goffé, B., Bousquet, R., Henry, P., Le Pichon, X., 2003. Effect of the chemical composition of the crust on
677 the metamorphic evolution of orogenic wedges. Journal of metamorphic geology 21(2), 123-141.

678 Groppo, C., Lombardo, B., Castelli, D., Compagnoni, R., 2007. Exhumation history of the UHPM
679 Brossasco-Isasca Unit, Dora-Maira Massif, as inferred from a phengite-amphibole eclogite.
680 International Geology Review 49(2), 142-168.

681 Guillot, S., Hattori, K.H., de Sigoyer, J., Nägler, T., Auzende, A.L., 2001. Evidence of hydration of the mantle
682 wedge and its role in the exhumation of eclogites. Earth and Planetary Science Letters 193, 115–127.

683 Guillot, S., Hattori, K., Agard, P., Schwartz, S., Vidal, O., 2009a. Exhumation Processes in Oceanic and
684 Continental Subduction Contexts: A Review, Springer, Berlin.

685 Guillot, S., di Paola, S., Ménot, R. P., Ledru, P., Spalla, M. I., Gosso, G., Schwartz, S., 2009b. Suture zones
686 and importance of strike-slip faulting for Variscan geodynamic reconstructions of the External
687 Crystalline Massifs of the western Alps. Bulletin de la Société Géologique de France 180(6), 483-500.

688 Hacker, B. R., Abers, G. A., 2004. Subduction Factory 3: An Excel worksheet and macro for calculating the
689 densities, seismic wave speeds, and H2O contents of minerals and rocks at pressure and temperature.
690 Geochemistry, Geophysics, Geosystems 5(1).

691 Hacker, B.R., Abers, G.A, Peacock, S.M., 2003. Subduction factory 1. Theoretical mineralogy, densities,
692 seismic wave speeds, and H_2O contents. Journal of Geophysical Research: Solid Earth 108 (B1).

693 Hacker, B.R., McClelland, W.C., Liou J.G. (Eds.), 2006. Ultrahigh-pressure metamorphism: Deep
694 continental subduction, Special Paper Geological Society of America 403, 206 pp.

695 Hacker, B. R., Kelemen, P. B., Behn, M. D., 2015. Continental lower crust. Annual Review of Earth and
696 Planetary Sciences 43, 167-205.

697 Handy, M.R., Schmid, S.M., Bousquet, R., Kissling, E., Bernoulli, D., 2010. Reconciling plate-tectonic
698 reconstructions of Alpine Tethys with the geological–geophysical record of spreading and subduction
699 in the Alps. Earth-Science Reviews 102(3), 121-158.

700 Hattori, K.H., Guillot, S., 2007. Geochemical character of serpentinites associated with high- to ultrahigh-
701 pressure metamorphic rocks in the Alps, Cuba, and the Himalayas: Recycling of elements in
702 subduction zones, Geochemistry, Geophysics, Geosystems 8, Q09010, doi:10.1029/2007GC001594.

703 Henry, C., Michard, A., Chopin, C., 1993. Geometry and structural evolution of ultra-high pressure and high-
704 pressure rocks from the Dora-Maira massif, western Alps, Italy. Journal of Structural Geology 15,
705 965–981.

706 Hermann, J., 2003. Experimental evidence for diamond-facies metamorphism in the Dora-Maira massif.
707 Lithos 70(3), 163-182.

708 Hermann, J., Müntener, O., Scambelluri, M., 2000. The importance of serpentinite mylonites for subduction
709 and exhumation of oceanic crust. Tectonophysics 327(3), 225-238.

710 Hetényi, G., Cattin, R., Brunet, F., Bollinger, L., Vergne, J., Nábělek, J. L., Diament, M., 2007). Density
711 distribution of the India plate beneath the Tibetan plateau: Geophysical and petrological constraints on
712 the kinetics of lower-crustal eclogitization. Earth and Planetary Science Letters 264(1), 226-244.

713 Jamieson, R.A., Beaumont, C., 2013. On the origin of orogens. Geological Society of America Bulletin
714 125(11-12), 1671–1702.

715 Jolivet, L., Faccenna, C., Goffé, B., Burov, E., Agard, P., 2003. Subduction tectonics and exhumation of
716 high-pressure metamorphic rocks in the Mediterranean orogens. American Journal of Science 303(5),
717 353-409.

718 Jourdan, S., Bernet, M., Schwartz, S., Guillot, S., Tricart, P., Chauvel, C., Dumont, T., Montagnac, G.,
719 Bureau, S., 2012. Tracing the Oligocene-Miocene evolution of the Western Alps drainage divide with
720 pebble petrology, geochemistry, and Raman spectroscopy of foreland basin deposits. Journal of
721 Geology 120(6), 603–624.

722 Jourdan, S., Bernet, M., Tricart, P., Hardwick, E., Paquette, J. L., Guillot, S., Dumont, T., Schwartz, S.,
723 2013. Short-lived, fast erosional exhumation of the internal western Alps during the late early
724 Oligocene: Constraints from geothermochronology of pro-and retro-side foreland basin sediments,
725 Lithosphere 5(2), 211–225.

726 Keller, L.M., Hess, M., Fügenschuh, B., Schmid, S.M., 2005. Structural and metamorphic evolution of the
727 Camughera–Moncucco, Antrona and Monte Rosa units southwest of the Simplon line, Western Alps.
728 Eclogae Geologicae Helvetiae 98(1), 19-49.

729 Kienast, J.R., Pognante, U., 1988. Chloritoid-bearing assemblages in eclogitised metagabbros of the Lanzo
730 peridotite body (western Italian Alps). Lithos 21(1), 1–11.

731 Lafay, R., Deschamps, F., Schwartz, S., Guillot, S., Godard, M., Nicollet, C. 2013. High pressure
732 serpentinites, a trap and release system controlled by metamorphic conditions: Example from the
733 Piedmont zone of the western Alps. Chemical Geology 343, 38–54.

734 Lagabrielle, Y., Cannat, M., 1990. Alpine jurassic ophiolites resemble the modern central atlantic basement.
735 Geology 18, 319–322.

736 Lanari, P., Rolland, Y., Schwartz, S., Vidal, O. Guillot, S., Tricart, P., Dumont, T., 2014. P-T-t estimation of
737 deformation in low-grade quartz-feldspar bearing rocks using thermodynamic modeling and $^{40}Ar/^{39}Ar$
738 dating techniques: example of the Plan-de-Phasy shear zone unit (Briançonnais Zone, Western Alps).
739 Terra Nova 26, 130–138.

740 Lardeaux, J.M., Schwartz, S., Tricart, P., Paul, A., Guillot, S., Béthoux, N., Masson, F., 2006. A crustal-scale
741 cross-section of the south-western Alps combining geophysical and geological imagery. Terra Nova
742 18, 6, 412–422.

743 Lemoine, M., Bas, T., Arnaud-Vanneau, A., Arnaud, H., Dumont, T., Gidon, M., Bourbon, M., De
744 Graciansky, P.C., Rudckiewicz, J.L., Megard-Galli, J., Tricart, P., 1986. The continental margin of the
745 Mesozoic Tethys in the Western Alps. Marine Petroleum Geology 3, 179–199.

746 Lenze, A., Stöckhert, B., 2007. Microfabrics of UHP metamorphic granites in the Dora Maira Massif, western
747 Alps – no evidence of deformation at great depth. Journal of Metamorphic Geology 25(4), 461–475.

748 Liou, J. G., Ernst, W. G., Zhang, R. Y., Tsujimori, T., Jahn, B. M., 2009. Ultrahigh-pressure minerals and
749 metamorphic terranes–the view from China. Journal of Asian Earth Sciences 35(3), 199-231.

750 Little, T. A., Hacker, B. R., Gordon, S. M., Baldwin, S. L., Fitzgerald, P. G., Ellis, S., Korchinski, M., 2011.
751 Diapiric exhumation of Earth's youngest (UHP) eclogites in the gneiss domes of the D'Entrecasteaux
752 Islands, Papua New Guinea. Tectonophysics 510(1), 39-68.

753 Liu, Y.H., Yang, H.,J., Takazawa, E., Satish-Kumar, M., You, C.F., 2015. Decoupling of the Lu-Hf, Sm-Nd,
754 and Rb-Sr isotope systems in eclogites and a garnetite from the Sulu ultra-high pressure metamorphic
755 terrane: Causes and implications. Lithos 234, 1–14.

756 Lombardo, B., Nervo, R., Compagnoni, R., Messiga, B., Kienast, J.R., Mével, C., Fiora, L., Piccardo, G.B.,
757 Lanza, R., 1978, Osservazioni preliminari sulle ofiolite metamorfiche del Monviso (Alpi Occidentali).
758 Rendiconti della Società Italiana di Mineralogia e Petrologia 34, 253–305.

759 Lyu, C., Pedersen, H., Paul, A., Zhao, L., Solarino, S. and the CIFALPS Working Group, 2017. Shear wave
760 velocities in the upper mantle of the Western Alps: new constraints using array analysis of seismic
761 surface waves. Geophysical Journal International, doi : 10.1093/gji/ggx166.

762 Malusà, M. G., Balestrieri, M. L., 2012. Burial and exhumation across the Alps–Apennines junction zone
763 constrained by fission-track analysis on modern river sands. Terra Nova 24(3), 221-226.

764 Malusà, M., Mosca, P., Borghi, A., Dela Pierre, F., Polino, R., 2002. Approccio multidisciplinare per la
765 ricostruzione dell'assetto tettono-stratigrafico e dell'evoluzione metamorfico-strutturale di un settore di
766 catena orogenica: l'esempio dell'Alta Valle di Susa (Alpi occidentali). Memorie della Società
767 Geologica Italiana 57(2), 249-257.

768 Malusà, M.G., Polino, R., Martin, S., 2005a. The Gran San Bernardo nappe in the Aosta valley (western
769 Alps): a composite stack of distinct continental crust units. Bulletin de la Société géologique de France
770 176(5), 417-431.

771 Malusà, M.G., Polino, R., Zattin, M., Bigazzi, G., Martin, S., Piana, F., 2005b. Miocene to Present differential
772 exhumation in the Western Alps: Insights from fission track thermochronology. Tectonics 24(3).

773 Malusà, M.G., Polino, R., Zattin, M., 2009. Strain partitioning in the axial NW Alps since the Oligocene.
774 Tectonics 28, TC3005, 1-26, doi:10.1029/2008TC002370.

775 Malusà, M.G., Faccenna, C., Garzanti, E., Polino, R., 2011. Divergence in subduction zones and exhumation
776 of high-pressure rocks (Eocene Western Alps). Earth and Planetary Science Letters 310, 21–32.

777 Malusà, M.G., Faccenna, C., Baldwin, S.L., Fitzgerald, P.G., Rossetti, F., Balestrieri, M.L., Danišík, M.,
778 Ellero, A., Ottria, G., Piromallo, C., 2015. Contrasting styles of (U)HP rock exhumation along the
779 Cenozoic Adria-Europe plate boundary (Western Alps, Calabria, Corsica). Geochemistry, Geophysics,
780 Geosystems 16(6), 1786–1824.

781 Malusà, M.G., Danišík, M., Kuhlemann, J., 2016a. Tracking the Adriatic-slab travel beneath the Tethyan
782 margin of Corsica-Sardinia by low-temperature thermochronometry. Gondwana Research 31, 135-149.

783 Malusà, M.G., Anfinson, O.A., Dafov, L.N., Stockli, D.F., 2016b. Tracking Adria indentation beneath the
784 Alps by detrital zircon U-Pb geochronology: Implications for the Oligocene–Miocene dynamics of the
785 Adriatic microplate. Geology 44(2), 155-158.

786 Malusà, M.G., Zhao, L., Eva, E., Solarino, S., Paul, A., Guillot, S., Schwartz, S., Dumont, T., Aubert, C.,
787 Salimbeni, S., Pondrelli, S., Wang Q., Zhu, R., 2017. Earthquakes in the western alpine mantle wedge.
788 Gondwana Research 44, 89–95.

789 Marschall, H. R., Schumacher, J. C., 2012. Arc magmas sourced from mélange diapirs in subduction zones.
790 Nature Geoscience 5(12), 862-867.

791 Mechie, J., Yuan, X., Schurr, B., Schneider, F., Sippl, C., Ratschbacher, L., Minaev, V., Gadoev, M.,
792 Oimahmadov, I., Abdybachaev, U., Moldobekov, B., Orunbaev, S., Negmatullaev, S., 2012. Crustal and
793 uppermost mantle velocity structure along a profile across the Pamir and southern Tien Shan as derived
794 from project TIPAGE wide-angle seismic data. Geophysical Journal International 188(2), 385-407.

795 Michard, A., Chopin, C., Henry, C., 1993. Compression versus extension in the exhumation of the Dora
796 Maira coesite-bearing unit, Western Alps, Italy. Tectonophysics 221, 173–193.

797 Michard, A., Avigad, D., Goffé, B., Chopin, C., 2004. The high-pressure metamorphic front of the south
798 Western Alps (Ubaye-Maira transect, France, Italy). Schweiz. Mineral. Petrogr. Mitt. 84, 215-235.

799 Müntener, O., Pettke, T., Desmurs, L., Meier, M., Schaltegger, U., 2004. Refertilisation of mantle peridotite
800 in embryonic ocean basins: trace element and Nd isotopic evidence and implications for crust mantle
801 relationships. Earth and Planetary Science Letters 221, 293–308.

802 Nagel, T.J., 2008. Tertiary subduction, collision and exhumation recorded in the Adula nappe, central Alps.
803 Geological Society, London, Special Publications 298, 365-392.

804 Nicolas, A., Hirn, A., Nicolich, R., Polino, R., 1990. Lithospheric wedging in the western Alps inferred from
805 the ECORS-CROP traverse. Geology 18, 587–590.

806 Paquette, J. L., Montel, J. M., Chopin, C., 1999. U-Th-Pb dating of the Brossasco ultrahigh-pressure
807 metagranite, Dora-Maira massif, western Alps. European journal of mineralogy 11(1), 69–77.

808 Paul, A., Cattaneo, M., Thouvenot, F., Spallarossa, D., Béthoux, N., Fréchet, J., 2001. A three-dimansional
809 crustal velocity model of the southwestern Alps from local earthquake tomography. Journal of
810 Geophysical Research 106(B9), 19367-19389.

811 Perrone, G., Eva, E., Solarino, S., Cadoppi, P., Balestro, G., Fioraso, G., Tallone, S., 2010. Seismotectonic
812 investigations in the inner Cottian Alps (Italian Western Alps): an integrated approach.
813 Tectonophysics 496(1), 1–16.

814 Petersen, K.D., Buck, W.R., 2015. Eduction, extension, and exhumation of ultrahigh-pressure rocks in
815 metamorphic core complexes due to subduction initiation. Geochemistry, Geophysics, Geosystems
816 16(8), 2564-2581.

817 Piccardo, G.B., Müntener, O., Zanetti, A., Pettke, T., 2004. Ophiolitic peridotites of the Alpine-Apennine
818 system: mantle processes and geodynamic relevance. International Geology Review 46 (12), 1119-1159.

819 Piccardo, G.B., Zanetti, A., Müntener, O., 2007. Melt/peridotite interaction in the Southern Lanzo peridotite:
820 field, textural and geochemical evidence. Lithos 94(1), 181–209.

821 Plümper, O., John, T., Podladchikov, Y.Y., Vrijmoed, J.C., Scambelluri, M., 2017. Fluid escape from
822 subduction zones controlled by channel-forming reactive porosity. Nature Geoscience 10, 150-156.

823 Quaranta, F., Piazza, M., Vannucci, G., 2009. Climatic and tectonic control on the distribution of the Oligocene
824 reefs of the Tertiary Piedmont Basin (NW Italy). Italian Journal of Geosciences 128(2), 587–591.

825 Quick, J. E., Sinigoi, S., Mayer, A., 1994. Emplacement dynamics of a large mafic intrusion in the lower
826 crust, Ivrea-Verbano Zone, northern Italy. Journal of Geophysical Research: Solid Earth 99(B11),
827 21559-21573.

828 Reynard, B., 2013. Serpentine in active subduction zones. Lithos 178, 171–185.

829 Rubatto, D., Hermann, J., 2001. Exhumation as fast as subduction ? Geology 29(1), 3–6.

830 Rubatto, D., Hermann, J., 2003. Zircon formation during fluid circulation in eclogites (Monviso, Western
831 Alps): implications for Zr and Hf budget in subduction zones. Geochimica et Cosmochimica Acta
832 67(12), 2173–2187.

833 Rubatto, D., Müntener, O., Barnhoorn, A., Gregory, C., 2008. Dissolution-reprecipitation of zircon at low-
834 temperature high-pressure conditions (Lanzo Massif, Italy). American Mineralogist 93, 1519–1529.

835 Rudnick, R. L., Fountain, D. M., 1995. Nature and composition of the continental crust: a lower crustal
836 perspective. Reviews of Geophysics 33, 267-309.

837 Scafidi, D., Solarino, S., Eva, C., 2006. Structure and properties of the Ivrea body and of the Alps-Apennines
838 systems as revealed by local earthquake tomography. Bollettino Geofisica Teorica Applicata 47, 497–514.

839 Scafidi, D., Solarino, S., Eva C., 2009. P wave seismic velocity and Vp/Vs ratio beneath the Italian Peninsula
840 from local earthquake tomography. Tectonophysics 465, 1–23.

841 Scambelluri, M., Tonarini, S., 2012. Boron isotope evidence for shallow fluid transfer across subduction
842 zones by serpentinized mantle. Geology 40, 907–910.

843 Scambelluri, M., Müntener, O., Hermann, J., Piccardo, G.B., Trommsdorff, V., 1995. Subduction of water
844 into the mantle: history of an Alpine peridotite. Geology 23, 459–462

845 Scambelluri, M., van Roermund, H. L., Pettke, T., 2010. Mantle wedge peridotites: fossil reservoirs of deep
846 subduction zone processes: inferences from high and ultrahigh-pressure rocks from Bardane (Western
847 Norway) and Ulten (Italian Alps). Lithos 120(1), 186-201.

848 Schaltegger, U., Brack, P., 2007. Crustal-scale magmatic systems during intracontinental strike-slip
849 tectonics: U, Pb and Hf isotopic constraints from Permian magmatic rocks of the Southern Alps.
850 International Journal of Earth Sciences 96(6), 1131–1151.

851 Schmid, S.M., Kissling, E., 2000. The arc of the western Alps in the light of geophysical data on deep crustal
852 structure. Tectonics 19, 62–85.

853 Schmid, S. M., Fügenschuh, B., Kissling, E., Schuster, R., 2004. Tectonic map and overall architecture of the
854 Alpine orogen. Eclogae Geologicae Helvetiae 97, 93-117.

855 Schmid, S.M., Kissling, E., Diehl, T., van Hinsbergen, D., Molli, G., 2017. Ivrea mantle wedge, arc of the
856 Western Alps, and kinematic evolution of the Alps–Apennines orogenic system. Swiss Journal of
857 Geosciences 110, 581-612.

858 Schwartz, S., Lardeaux, J.M., Guillot, S., Tricart, P., 2000. Diversité du métamorphisme éclogitique dans le
859 massif ophiolitique du Monviso (Alpes occidentales, Italie). Geodinamica Acta 13, 169-188.

860 Schwartz, S., Allemand, P., Guillot, S. 2001. Numerical model of the effect of serpentinites on the
861 exhumation of eclogitic rocks: insights from the Monviso ophiolitic massif (Western Alps).
862 Tectonophysics 342, 193–206.

863 Schwartz, S., Tricart, P., Lardeaux, J.M., Guillot, S., Vidal, O. 2009. Late tectonic and metamorphic
864 evolution of the Piedmont accretionary wedge (Queyras Schistes lustrés, western Alps): Evidences for
865 tilting during Alpine collision. Geological Society of America Bulletin 121, 502–518.

866 Schwartz,, S., Gautheron, C., Audin, L., Dumont, T., Nomade, J., Barbarand, J., 2017. Foreland exhumation
867 controlled by crustal thickening in the Western Alps. Geology 45(2), 139–142.

868 Solarino, S., Kissling, E., Sellami, S., Smriglio, G., Thouvenot, F., Granet, M., Bonjer, K.P., Slejko, D.,
869 1997. Compilation of a recent seismicity data base of the greater Alpine region from several
870 seismological networks and preliminary 3D tomographic results. Annals of Geophysics 40(1).

871 Sue, C., Delacou, B., Champagnac, J.D., Allanic, C., Tricart, P., Burkhard, M., 2007. Extensional
872 neotectonics around the bend of the Western/Central Alps: an overview. International Journal of Earth
873 Sciences 96(6), 1101-1129.

874 Thurber, C.H., 1983. Earthquake locations and three-dimensional crustal structure in the Coyote Lake area,
875 central California. Journal of Geophysical Research: Solid Earth 88(B10), 8226–8236.

876 Tricart, P., Schwartz, S., 2006. A north - south section across the Queyras Schistes lustrés (Piedmont zone,
877 Western Alps) : syncollision refolding of a subduction wedge. Eclogae Geologicae Helvetiae 9, 429–442.

878 Tricart, P., Schwartz, S., Sue, C., Lardeaux, J.M., 2004. Differential exhumation in the inner western Alpine
879 arc evidenced by late normal faulting (eastern Queyras Schistes lustrés). Journal of Structural Geology
880 26, 1633–1645.

881 Tricart, P., van der Beek, P., Schwartz, S., Labrin, E., 2007. Diachronous late-stage exhumation across the
882 western Alpine arc: constraints from apatite fission-track thermochronology between the Pelvoux and
883 Dora-Maira Massifs. Journal of the Geological Society 164(1), 163-174.

884 Vernon, A.J., van der Beek, P.A., Sinclair, H.D., Rahn, M.K., 2008. Increase in late Neogene denudation of
885 the European Alps confirmed by analysis of a fission-track thermochronology database. Earth and
886 Planetary Science Letters 270, 316–329.

887 Vignaroli, G., Faccenna, C., Jolivet, L., Piromallo, C., Rossetti, F. (2008). Subduction polarity reversal at the
888 junction between the Western Alps and the Northern Apennines, Italy. Tectonophysics 450(1), 34-50.

889 Virieux, J., 1991. Fast and accurate ray tracing by Hamiltonian perturbation. Journal of Geophysical
890 Research: Solid Earth 96(B1), 579–594.

891 van Roermund, H. (2009). Mantle-wedge garnet peridotites from the northernmost ultra-high pressure domain
892 of the Western Gneiss Region, SW Norway. European Journal of Mineralogy 21(6), 1085-1096.

893 Wagner, M., Kissling, E., Husen, S., 2012. Combining controlled-source seismology and local earthquake
894 tomography to derive a 3-D crustal model of the western Alpine region. Geophysical Journal
895 International 191(2), 789–802.

896 Wang, Q., Ji, S., Salisbury, M. H., Xia, B., Pan, M., Xu, Z., 2005. Pressure dependence and anisotropy of P-
897 wave velocities in ultrahigh-pressure metamorphic rocks from the Dabie–Sulu orogenic belt (China):
898 implications for seismic properties of subducted slabs and origin of mantle reflections. Tectonophysics
899 398(1), 67–99.

900 Warren, C.J., 2013. Exhumation of (ultra-) high-pressure terranes: Concepts and mechanisms. Solid Earth
901 4(1), 75–92.

902 Weiss, T., Siegesmund, S., Rabbel, W., Bohlen, T., Pohl, M., 1999. Seismic velocities and anisotropy of the
903 lower continental crust. A Review. Pure Applied Geophysics 156, 97–122.

904 Yamato, P., Burov, E., Agard, P., Le Pourhiet, L., Jolivet, L., 2008. HP-UHP exhumation during slow
905 continental subduction: Self-consistent thermodynamically and thermomechanically coupled model
906 with application to the Western Alps. Earth and Planetary Science Letters 271(1), 63-74.

907 Zanchetta, S., Malusà, M.G., Zanchi, A., 2015. Precollisional development and Cenozoic evolution of the
908 Southalpine retrobelt (European Alps). Lithosphere 7, 662-681.

909 Zeitler, P.K., Koons, P.O., Bishop, M.P., Chamberlain, C.P., Craw, D., et al., 2001. Crustal reworking at
910 Nanga Parbat, Pakistan: metamorphic consequences of thermal–mechanical coupling facilitated by
911 erosion, Tectonics, 20, 712–728.

912 Zhao, L., Paul, A., Guillot, S., Solarino, S., Malusà, M.G., Zheng, T., Aubert, C., Salimbeni, S., Dumont, T.,
913 Schwartz, S., Zhu, R., Wang, Q., 2015. First seismic evidence for continental subduction beneath the
914 Western Alps. Geology 43, 815-818.

915 Zhao, L., Paul, A., Malusà, M.G., Xu, X., Zheng, T., Solarino, S., Guillot, S., Schwartz, S., Dumont, T.,
916 Salimbeni, S., Aubert, C., Pondrelli, S., Wang, Q., Zhu, R., 2016a. Continuity of the Alpine slab
917 unraveled by high-resolution P wave tomography. Journal of Geophysical Research: Solid Earth 121,
918 8720–8737.

919 Zhao, L., Paul, A., Solarino S., 2016b. Seismic network YP: CIFALPS temporary experiment (China-Italy-
920 France Alps seismic transect). RESIF - Réseau Sismologique et géodésique Français. Seismic
921 Network. doi:10.15778/RESIF.YP2012.

922 Zhao, L., Xu, X., Malusà, M.G., 2017. Seismic probing of continental subduction zones. Journal of Asian
923 Earth Sciences 145, 37-45.
924

Figure 1

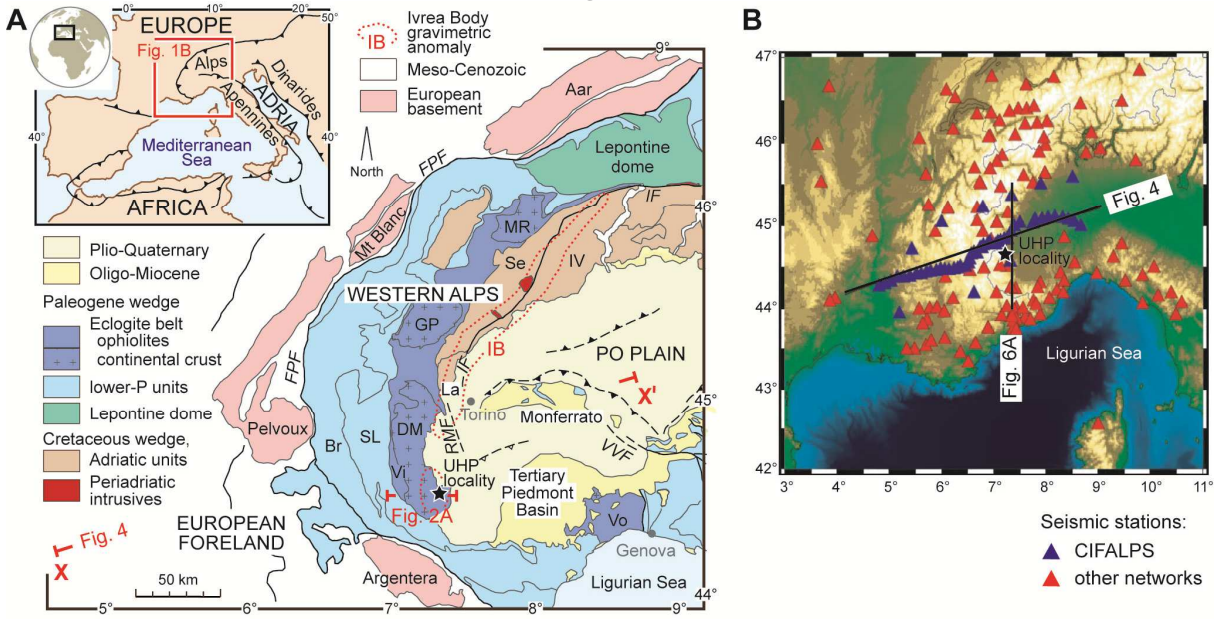

Figure 1: A) Tectonic sketch map showing the (U)HP domes of the Western Alps (dark blue), the gravimetric anomaly of the Ivrea body (0 mGal isoline in red), and the location of the CIFALPS transect (X-X'). Acronyms: Br, Briançonnais; DM, Dora-Maira; FPF, Frontal Pennine Fault; GP, Gran Paradiso; IF, Insubric Fault; IV, Ivrea-Verbano; La, Lanzo; MR, Monte Rosa; RMF, Rivoli-Marene deep fault; Se, Sesia-Lanzo; SL, Schistes lustrés; Vi, Viso; Vo, Voltri; VVF, Villalvernia-Varzi Fault. The black star marks the Brossasco-Isasca UHP locality. B) Seismic stations utilized in this work (blue = CIFALPS; red = other networks) and location of tomographic cross sections (black lines).

Figure 2

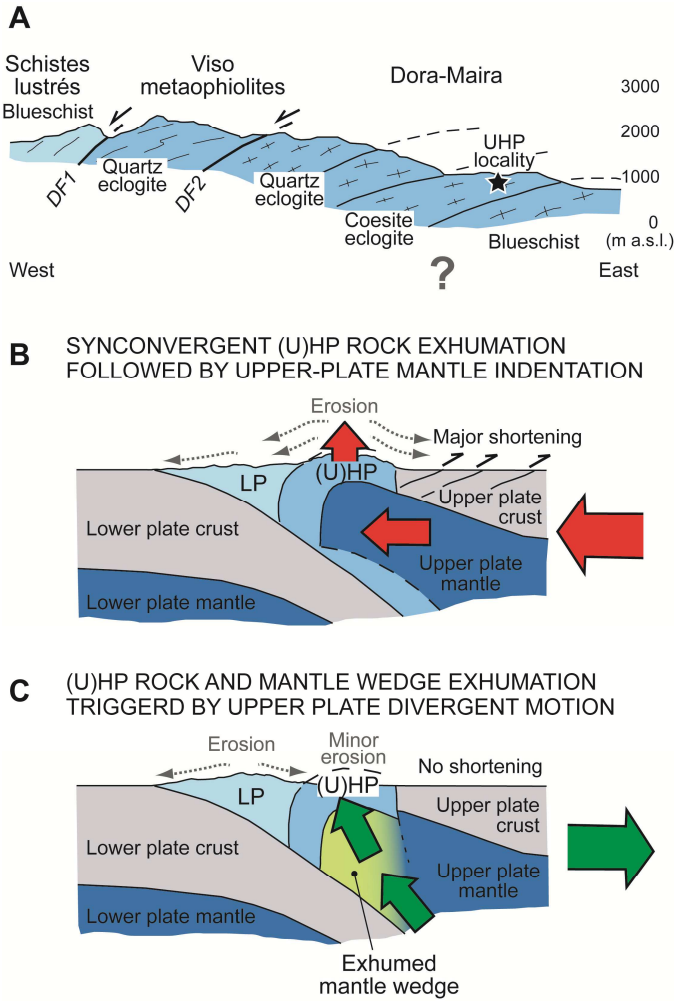

Figure 2: **A)** Geologic cross-section of the Dora-Maira (U)HP dome (see location in Fig. 1A; based on Avigad et al., 2003; Lardeaux et al., 2006). **B, C)** Alternative scenarios of mantle involvement in (U)HP orogenic belts. In (B), synconvergent exhumation of (U)HP rocks (e.g., Butler et al., 2013), possibly associated with deep duplex formation (Schmid et al., 2017), is followed by indentation of the upper-plate mantle beneath the accretionary wedge, with consequent fast erosion of the (U)HP dome and major tectonic shortening in the upper plate (e.g., Béthoux et al., 2007). Seismic velocities in the upper-plate mantle are similar beneath the orogenic belt and in the hinterland, as indicated by the uniform dark blue colour. In (C), divergence between upper plate and accretionary wedge triggers the exhumation of (U)HP rocks (Malusà et al., 2011) and the emplacement of serpentinized mantle-wedge rocks at shallow depth. Erosion on top of the (U)HP dome is minor at this stage, and shortening is negligible. Because of widespread serpentinization of the mantle wedge during subduction, seismic velocities will be lower in the mantle-wedge rocks beneath the (U)HP dome (as indicated by the pale green colour), and higher in the adjoining dry mantle rocks of the upper plate (dark blue).

Figure 3

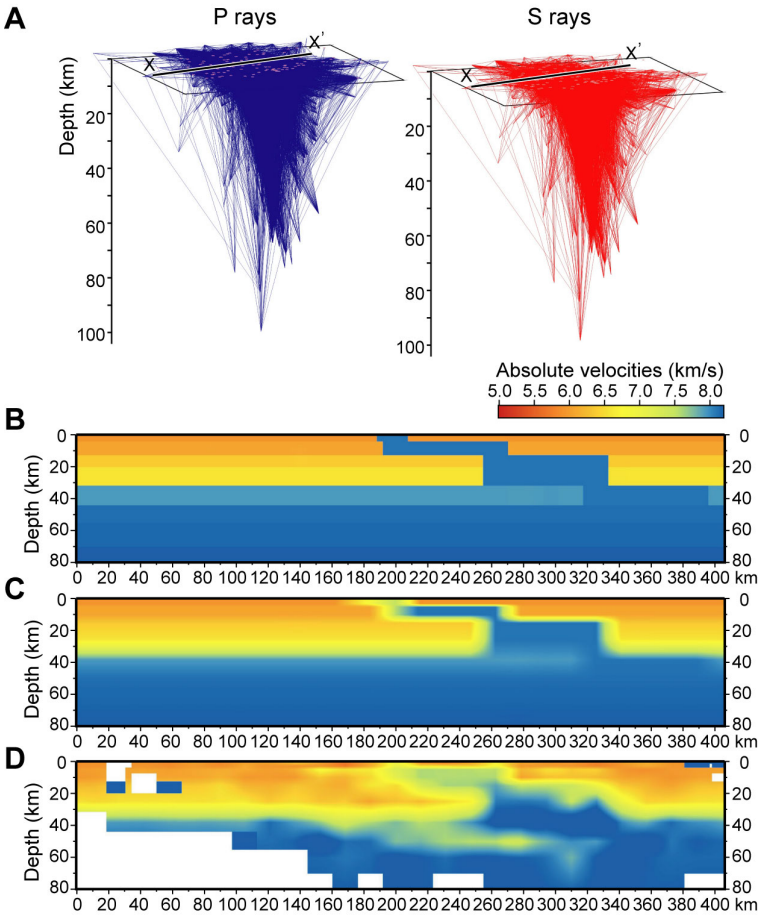

Figure 3. A) Three-dimensional P and S ray coverage based on the seismic events considered in this study (X-X' indicates the CIFALPS transect, see Fig. 1). B) Imposed stairwell geometry along the CIFALPS transect for testing the resolution capability of the coupling between seismic dataset and inversion setup. C) Same geometry after interpolation by the algorithm used in SIMULPS, which introduces a smoothing and a thin band of fake colors around the anomalies. D) Reconstruction test showing that the shape of the imposed stairwell structure is well reproduced using our dataset, but the high velocities in the uppermost 10 km are converted to lower values (as less as 0.5 km/s); the weak vertical and horizontal periodic stripes of yellow color at 50 km depth within the blue area are artifacts; white areas are not sampled.

Figure 4

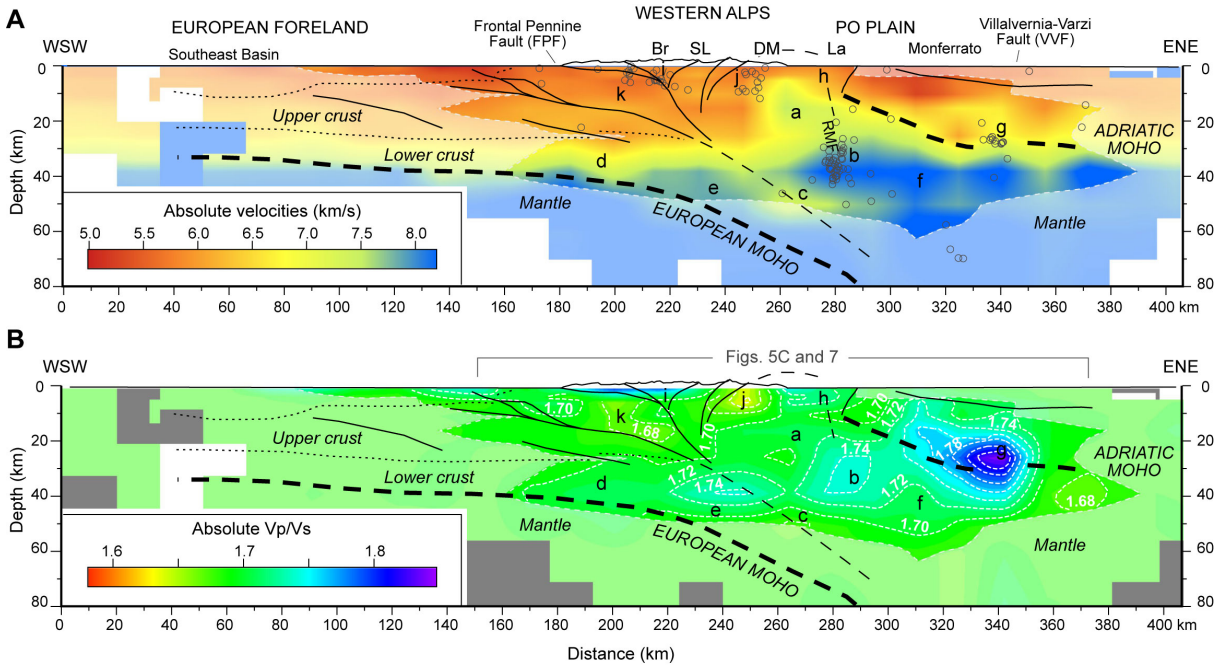

Figure 4: Tomographic cross sections along the CIFALPS transect. A) Absolute Vp velocity. The velocity structure beneath the Dora-Maira (U)HP dome is well resolved down to 50-60 km depth (acronyms as in Fig. 1A); areas with resolution diagonal elements <0.1 are masked, white areas are not sampled; letters a to k indicate regions of the model discussed in the main text; black circles indicate earthquakes as located with the 3D model; black lines and text in italics indicate the main tectonic features previously inferred from receiver function analysis (Zhao et al., 2015; Malusà et al., 2017, see Fig. 7B). Note the prominent high velocity body (labelled with "a") located right below the Dora-Maira (U)HP dome. The vertical and horizontal periodic stripes of yellow color at 50 km depth are artifacts, as attested by the reconstruction test of Fig. 3D. B) Vp/Vs ratios. White dashed lines are isolines of equal Vp/Vs, grey areas are not sampled (other keys as in frame A).

Figure 5

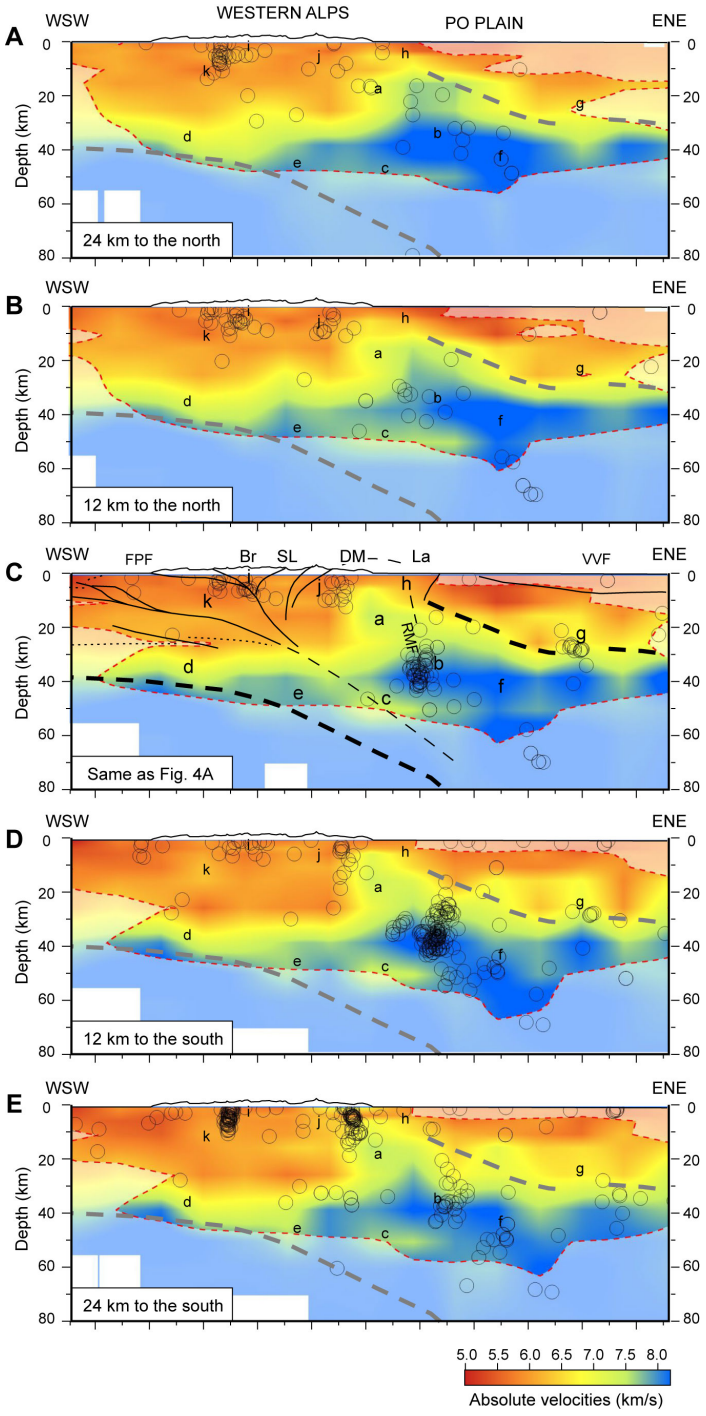

Figure 5: Lateral variations in Vp velocity in the mantle wedge as shown in a series of WSW-ENE cross-sections lying to the north (A, B) and to the south (D, E) of the main CIFALPS transect (C). The high velocity body labelled with "a" progressively disappears moving to the north. Black circles are projected hypocentres located within ±5 km distance off the profiles. The thick dashed lines, reported in all sections for comparison, indicate the European and Adriatic Mohos inferred from receiver function analysis (cf. Fig. 7B). Other keys as in Fig. 4.

Figure 6

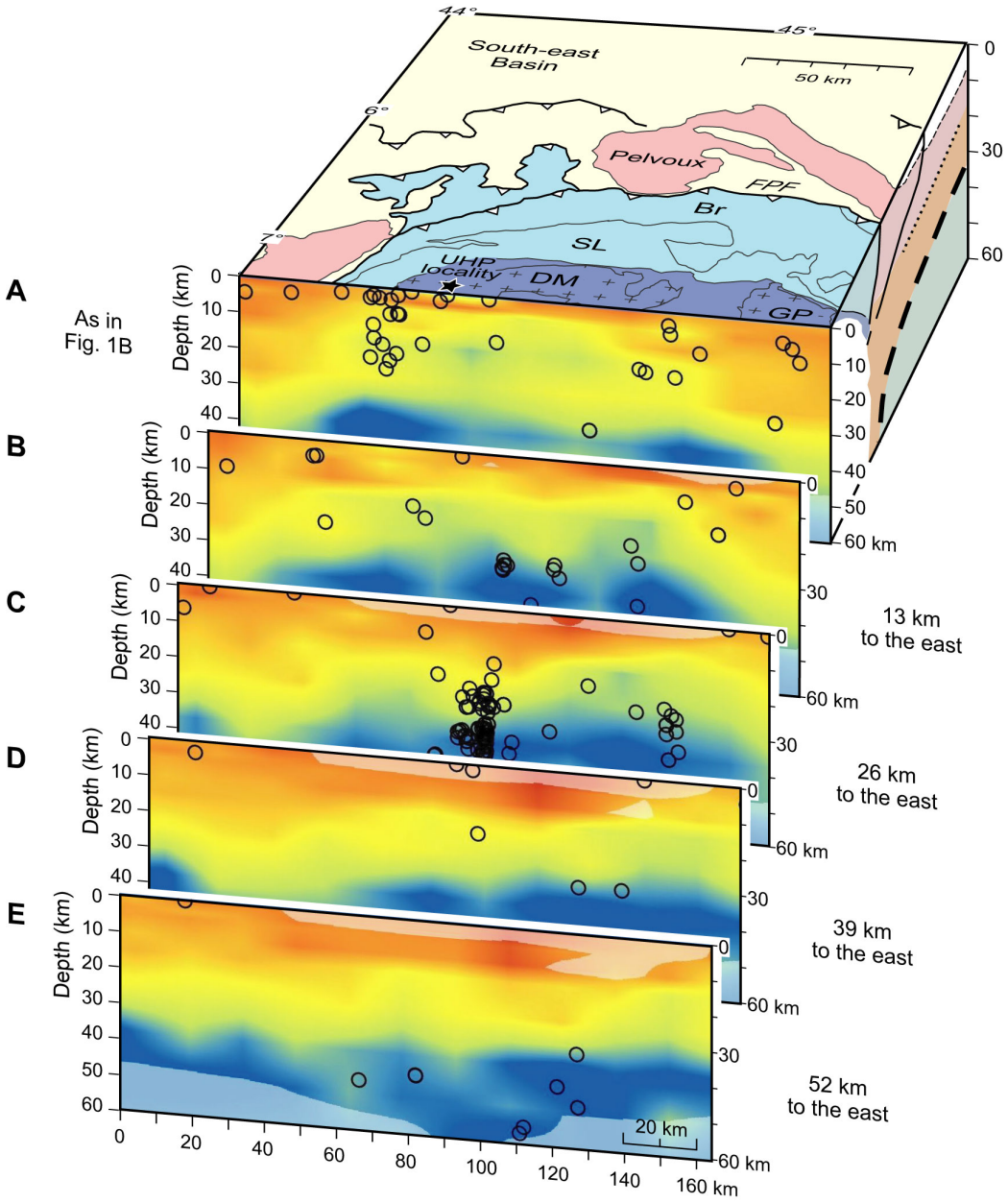

Figure 6: Lateral variations in Vp velocity beneath the Dora-Maira (U)HP dome, as shown in a series of N-S cross-sections from the mountain range to the Po Plain. Black circles are projected hypocentres located within ±3 km distance off the profiles. The high-velocity body labelled with "a" in Figs. 4 and 5 is exclusively found beneath the Dora-Maira dome (see cross section A) and progressively disappears towards the east. Acronyms as in Fig. 1.

Figure 7

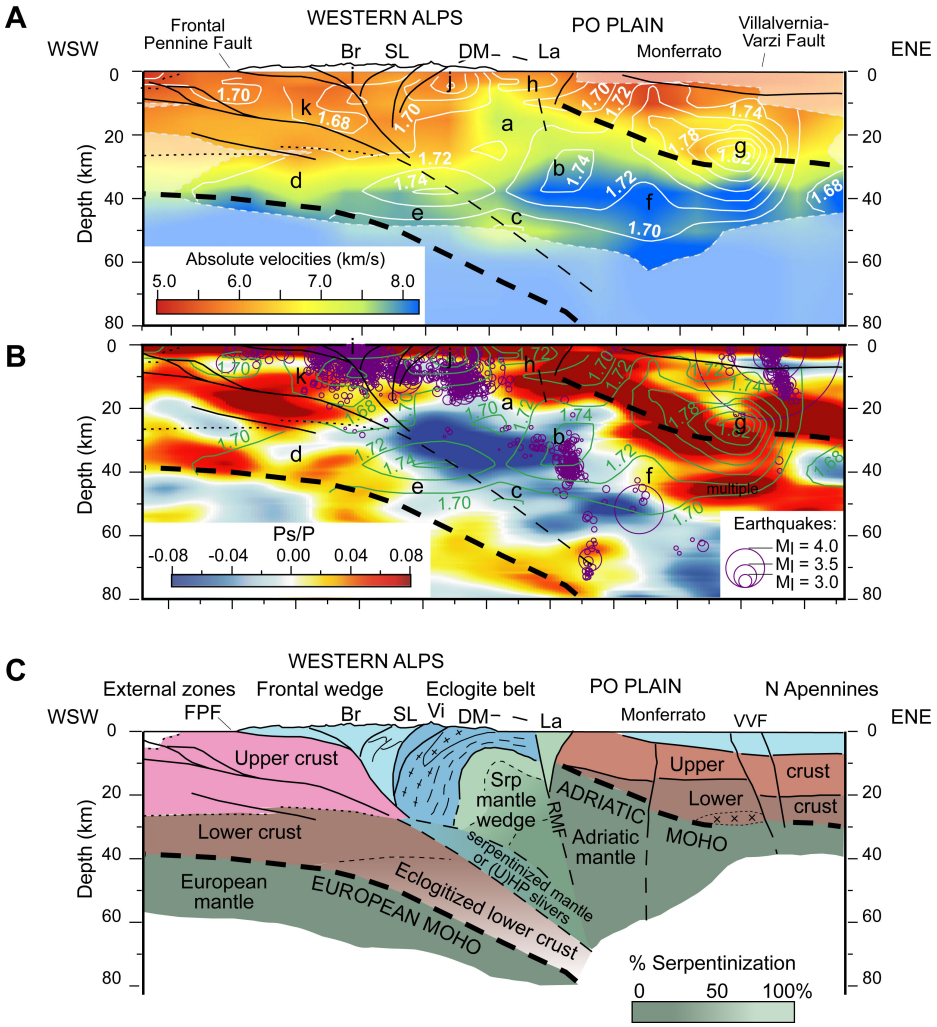

Figure 7: Synthesis of geophysical data (A, B) and inferred mantle wedge structure (C). Black lines in A and B are tectonic features based on receiver function analysis (colors in B indicate positive- and negative-polarity Ps-converted phases, Zhao et al., 2015); contours are isolines of equal Vp/Vs; purple circles in B are earthquakes recorded since 1990 (Malusà et al., 2017). The amount of serpentinization in C, in the mantle wedge underlying the Dora-Maira (U)HP dome, is inferred from seismic velocities (Reynard, 2013). Note the consistency between structures unravelled by local (A) and teleseismic (B) events. Acronyms as in Fig. 1, letters a to k as in Fig. 4.

Figure 8

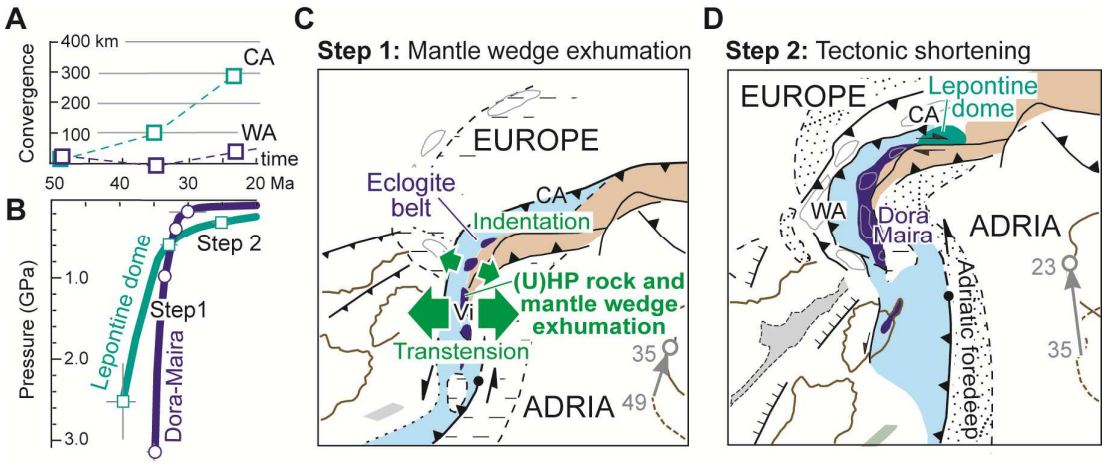

Figure 8: Geodynamic framework of mantle wedge exhumation. **A)** Trench-normal component of Adria-Europe relative motion in the Central (CA) and Western Alps (WA) segments of the Alpine subduction zone (Malusà et al., 2015). **B)** Pressure-time exhumation paths (Dora-Maira: Chopin et al., 1991; Rubatto and Hermann, 2001; Lepontine dome: Becker, 1993; Gebauer, 1996; Brouwer et al., 2004; Nagel, 2008). **C,D)** Late Eocene transtension leading to (U)HP rock and mantle wedge exhumation, and subsequent tectonic shortening in the early Oligocene; grey arrows indicate Adria motion relative to Europe (modified after Malusà et al., 2015).